Influence of a small submarine canyon on biogenic matter export flux in the Lower St. Lawrence Estuary, eastern Canada

Hannah Sharpe[1], Michel Gosselin[2], Catherine Lalande[3], Alexandre Normandeau[4], Jean-Carlos Montero-Serrano[2], Khouloud Baccara[2], Daniel Bourgault[2], Owen Sherwood[5], Audrey Limoges[1]

5   [1]Department of Earth Sciences, University of New Brunswick, Fredericton, E3B 5A3, Canada
[2]Institut des sciences de la mer de Rimouski, Université du Québec à Rimouski, Rimouski, G5L 2Z9, Canada
[3]Amundsen Science, Université Laval, Québec City, G1V 0A6, Canada
[4]Geological Survey of Canada (Atlantic), Bedford Institute of Oceanography, Dartmouth, B2Y 4A2, Canada
[5]Department of Earth and Environmental Sciences, Dalhousie University, Halifax, B3H 4R2, Canada

10   *Correspondence to*: Hannah Sharpe (hsharpe@unb.ca) and Audrey Limoges (alimoges@unb.ca)

Abstract. Submarine canyons enhance shelf-slope sediment exchange and influence hydrodynamic processes, with consequences for biogeochemical cycles. This work documents variations in the vertical export of biogenic matter on the northern shore of the Lower St. Lawrence Estuary (LSLE, Quebec, eastern Canada), which is characterized by the presence of an active submarine canyon system. A total of three moorings were deployed from November 2020 to

15   September 2021. One nearshore mooring was deployed in the main axis of the Pointe-des-Monts (PDM) canyon system and was equipped with an Acoustic Doppler Current Profiler (ADCP), and two moorings equipped with sediment traps were deployed in the distal PDM canyon system and offshore Baie-Comeau (BC). The ADCP data revealed the occurrence of a minor sediment remobilization event (December 2020) and a small turbidity current (February 2021) in the canyon. Concurrent elevated fluxes of total particulate matter, particulate organic carbon,

20   particulate nitrogen, and chloropigments showed that these events left a signature in the distal PDM sediment trap located >2.6 km further offshore. The composition of diatom and dinoflagellate assemblages was similar in the canyon system and offshore BC, but the diatom bloom occurred two weeks earlier (in mid-April) at the PDM site, where annual diatom and dinoflagellate fluxes were almost 2 times lower than at the BC site. A bloom of the potentially toxic diatom *Pseudo-nitzschia seriata* was also observed during the second half of September 2021 at the BC site.

25   This study notably helps identify the relationship between near-bed canyon processes and biogenic matter export in the water column, thereby directly influencing the regional ecosystem. The study period further covered an anomalously nearly ice-free winter and thus, in the context of climate change, provides valuable insight into future trends of biogenic matter export in the LSLE.

1 Introduction

30   Submarine canyons are erosional features that cut into the seabed of continental margins and slopes. Canyons are preferential particle-transport routes from the coast to deep depositional sinks, leading to important sites of sediment accumulation on submarine fans (Covault, 2011). Owing to their bathymetric complexity, large canyon systems are known to significantly influence hydrodynamic processes and induce shelf-slope exchanges of water and matter through turbidity currents, funneling of internal tides and waves, and enhanced downwelling and upwelling

35   currents, thereby playing a key role in biogeochemical cycling of elements and supporting biodiversity hotspots (Fernandez-Arcaya et al., 2017 and references therein; Paull et al., 2018; Santora et al., 2018).

The St. Lawrence Estuary (Quebec, eastern Canada), one of the largest and deepest estuaries in the world, supports several ecosystem services such as biodiversity, tourism, and fisheries. Located at the transition between the Lower St. Lawrence Estuary (LSLE) and the Gulf of St. Lawrence, the region of Pointe-des-Monts (PDM; Fig. 1)

40   hosts three small submarine canyons with lengths up to 3.5 km, widths of 100–300 m, and depths down to 300 m (Normandeau et al., 2015). These canyons are sediment-starved, meaning they have limited sediment input at their heads. Turbidity currents thus remobilize small volumes of sediment stored on the shelf and previously deposited deglacial and post-glacial sediment within the canyons. The processes leading to the formation of the canyons and storm-induced turbidity currents have been the subjects of previous studies (Normandeau et al., 2014, 2020, 2022).

45   However, despite the presence of the nearby Saguenay – St. Lawrence Marine Park, a National Marine Conservation Area (Fig. 1c), it is currently unknown whether the canyon's sedimentary and hydrodynamic processes influence regional primary production and biogenic matter export. Furthermore, while it is relatively well known that the complex hydrodynamics of large submarine canyons increase the occurrence of biodiversity hotspots (Fernandez-Arcaya et al., 2017; Paull et al., 2018; Santora et al., 2018), the same concept is not established for smaller systems, such as at PDM.

50   To address this gap, the present study investigates the seasonal and spatial variability in the magnitude and composition of biogenic matter export on the north shore of the LSLE using in situ measurements obtained from November 2020 to September 2021. Two sediment traps were strategically deployed at two depths over the submarine fan at the base of the PDM canyon system to characterize the biogenic matter sinking from the euphotic zone and

55   resuspended from the seafloor (Fig. 1d, e). To identify canyon-specific processes, a sediment trap was also deployed offshore Baie-Comeau (BC) to contrast with biogenic matter export in the LSLE (Fig. 1c). At PDM, the time-series biogenic matter fluxes were further compared to data obtained with a down-looking Acoustic Doppler Current Profiler (ADCP) installed in the axis of the main canyon (Fig. 1d, e). The ADCP also recorded data from November 2020 to September 2021 to determine if turbidity currents and other sediment remobilization events within the canyon

60   influenced biogenic matter fluxes and phytoplankton assemblages over the submarine fan located >2.6 km further offshore. Finally, sinking particles were examined for the presence of potentially harmful species of diatoms and dinoflagellates that may pose a threat to the LSLE ecosystem.
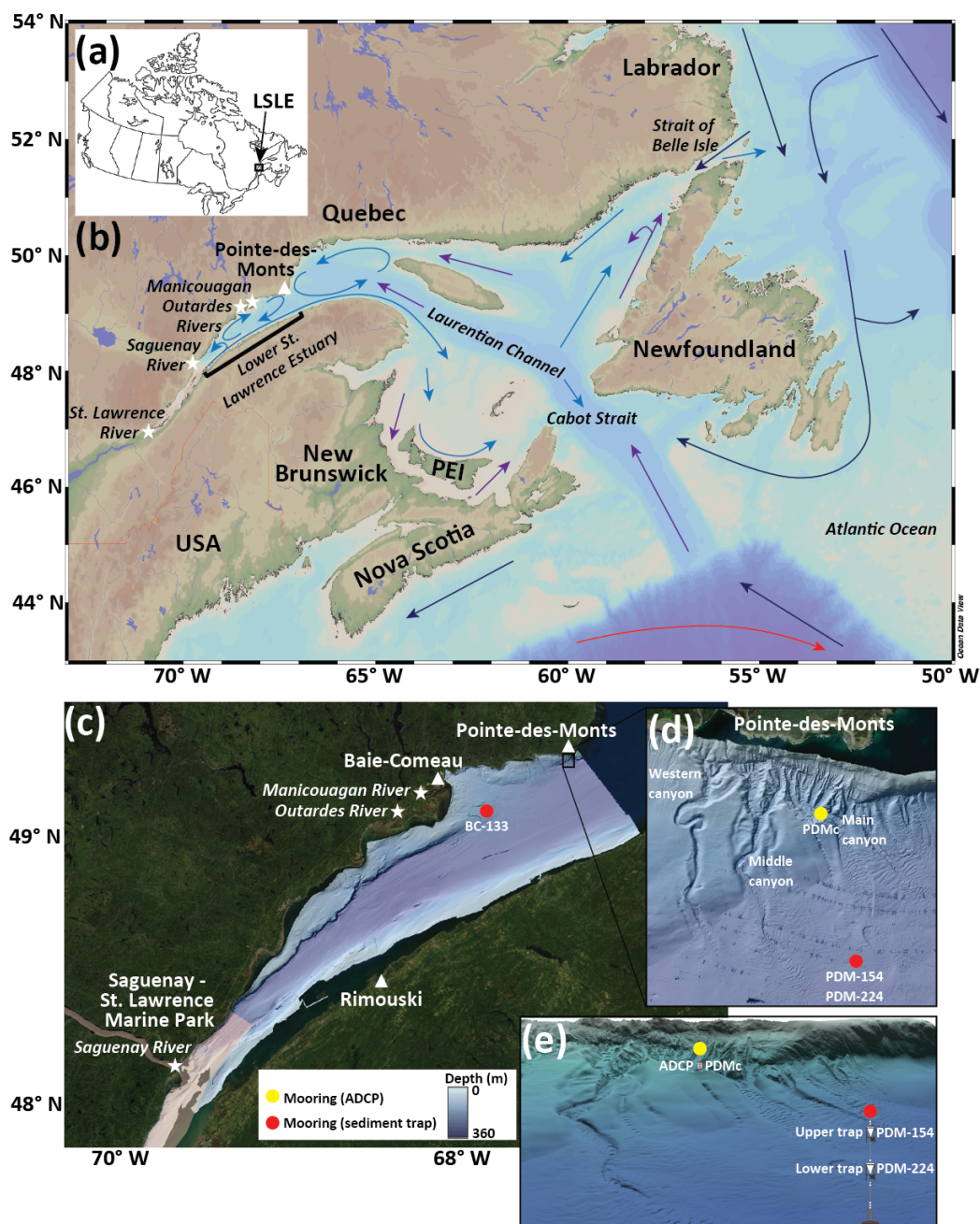
Figure 1: (a) Location of the Lower St. Lawrence Estuary (LSLE), eastern Canada. (b) Map of eastern Canada highlighting
the main patterns of surface (light blue) and deep-water circulation (purple), which is a combination of the Labrador
Current (dark blue) and the Gulf Stream (red). Circulation patterns are adapted from Weise et al. (2002), Bernier et al.
(2018), and Ryan et al. (2019). White stars represent the outlets of the major freshwater sources to the Lower St. Lawrence
Estuary and the white triangle highlights Pointe-des-Monts. (c-e) The Lower St. Lawrence Estuary with locations of
moorings equipped with sediment traps (red) and an Acoustic Doppler Current Profiler (yellow). The location of the
Saguenay-St. Lawrence Marine Park is highlighted in light pink. (d-e) Pointe-des-Monts submarine canyon system.

2 Regional setting

The LSLE is characterized by a seasonally-stratified three-layer water column that exhibits large spatial and temporal variability (Galbraith et al., 2022). The low salinity surface mixed layer (25 to 32 psu) flows seaward into

75 the Atlantic Ocean with the main sources of freshwater being the Saguenay, Outardes, and Manicouagan rivers located on the north shore, in addition to the St. Lawrence River (Fig. 1). The cold intermediate layer (-1 to 2°C, 31.5 to 33 psu) predominantly flows landward on the north shore and seaward on the south shore, with an overall net landward transport (Mucci et al., 2011). In the fall and winter, atmospheric cooling and intense vertical mixing, due to wind-driven mixing and brine rejection, cause the surface layer to gradually become cooler and deeper until it merges with

80 the cold intermediate layer (Gilbert and Pettigrew, 1997). The warmer deep layer (2 to 6°C, >33 psu) is a mixture of waters from the Labrador Current and the North Atlantic entering the Gulf of St. Lawrence via Cabot Strait (Dickie and Trites, 1983). The Labrador Current originates in the Arctic and contributes cold, fresh, oxygen-rich waters while the North Atlantic waters, originating from the Gulf Stream, are warm, saline, and oxygen-poor (Gilbert et al., 2005). The deep layer flows landward through the Laurentian Channel, a 1240 km glaciated trough which extends from the

85 edge of the eastern Canadian continental shelf to the mouth of the Saguenay River, where a sill causes the seabed to rise suddenly and lead to upwelling of bottom waters (Ingram, 1983).

Sea ice typically begins to form along the north shore of the LSLE in December. However, by mid-December 2020, sea-surface temperatures were above average, delaying the onset of sea ice formation by several weeks (Fig. 2). Sea ice cover has been declining since 1990, with record low sea ice conditions observed in 2010 followed by 2021,

90 and both years were classified as nearly ice-free (Galbraith et al., 2022). Thus, in the context of climate warming, high-resolution data collection during these anomalous years can provide valuable insight into future trends in the LSLE system.
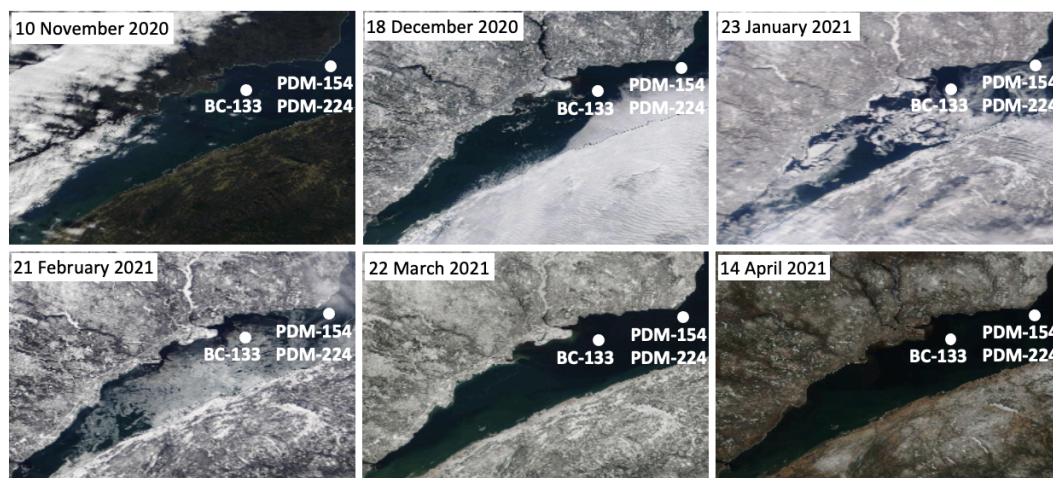
95 **Figure 2: Satellite images of the LSLE (EODIS Worldview) showing sea ice cover variability from November 2020 to April 2021.**

3 Methods

3.1 CTD-rosette and moorings

Water column profiles of temperature, salinity, in vivo chlorophyll fluorescence, and photosynthetically active radiation were obtained on board the research vessel *Coriolis II* at the BC and PDM mooring sites before mooring deployment on 15 October 2020. Data acquisition was done using a rosette sampler equipped with a conductivity, temperature, depth (CTD) probe (Sea-Bird Electronic SBE 911plus), an *in situ* fluorometer (Wet Labs ECO-AFL/FL), and a Chelsea scalar quantum irradiance sensor. The euphotic zone was determined based on the depth where the PAR value was 1% of its surface value. The depths of the surface mixed layer and cold intermediate layer were estimated based on the vertical gradient in temperature and salinity.

A total of three moorings were deployed in October 2020 and retrieved in October 2021. Two moorings were equipped with sediment traps (Technicap PPS 6/2; aspect ratio: 6.25; opening area: 0.5 m²) deployed at 133 m at the Baie-Comeau site (BC-133) and at 154 and 224 m at the Pointe-des-Monts site (PDM-154 and PDM-224; Fig. 1, Table 1). Traps BC-133 and PDM-224 were positioned 67 m and 58 m above seafloor, respectively. The sediment traps consisted of a funnel connected to a carousel holding with 24 sample cups (525 mL) programmed to rotate approximately every two weeks over an annual cycle with increased resolution in April. Prior to deployment, seawater was sequentially filtered through a 3 μm A/D glass fiber filter (Pall Corporation) and a 0.2 μm GTTP membrane filter to prepare the preservative solution for the sample cups. The cups were then filled with filtered seawater adjusted to a salinity >33 psu with NaCl, fixed with 37% formaldehyde (final concentration 5 % w/v formalin), and buffered with borax to preserve samples during deployment and after recovery (Hargrave et al., 2002). The last sample cup of each annual cycle was excluded from the analyses due to a technical error resulting in the cups remaining open upon recovery. After retrieval, all sample cups were kept at 4°C in the dark until biogenic matter analysis and cell identification. CTD and CT sensors attached to traps BC-133 and PDM-154 recorded water temperature and salinity at 15 min intervals from November 2020 to September 2021.

Table 1: Mooring deployments information.

	PDMc	BC-133	PDM-154, PDM-224
Deployment (d/m/yr)	14/10/2020	15/10/2020	15/10/2020
Recovery (d/m/yr)	11/10/2021	14/10/2021	11/10/2021
Latitude (°N)	49.30654	49.11802	49.284065
Longitude (°W)	67.39241	67.88304	67.38159
Sediment trap depth (m)	-	133	154, 224
ADCP depth (m)	156	-	-
ADCP sensor	Teledyne RDI Workhorse 600 kHz	-	-
CTD / CT depth (m)	-	133	154
CTD / CT sensor	-	SBE 37-SM MicroCAT with RS-232 Interface	SBE 16plus V2 SeaCAT
Water column depth (m)	183	200	282

A third mooring was deployed in the axis of the main PDM canyon (PDMc) at 183 m water depth (Fig. 1; Table 1). The PDMc mooring was equipped with a down-looking ADCP deployed at 156 m that recorded velocity, acoustic backscatter, and pressure once every 20 seconds with a vertical bin size of 1 m. The ADCP recorded all pings

ensemble averaging and the acoustic beams were at a 20° angle respective to a vertical line. The ADCP data were analyzed in conjunction with bathymetric data to monitor the occurrence of turbidity currents, smaller sediment remobilization events and hydrodynamic processes. To assess the relation between sediment remobilization and sinking particles, the average acoustic backscatter (dB) and the maximum daily average acoustic backscatter were

130 determined for each corresponding sediment trap sampling period.

3.2 Total particulate matter and geochemical signature

Prior to subsampling for all laboratory analyses, each sample cup was gently mixed for 100 seconds to ensure homogeneity before subsamples were collected using a pipette. For total particulate matter (TPM) measurements, triplicates of 1 to 3 mL were filtered onto 21 mm Whatman GF/F filters (nominal porosity of 0.7 μm) pre-combusted

135 at 450°C for 5 h and pre-weighed with a Mettler Toledo MX5 Microbalance. The filters were rinsed with 5 mL of Nanopure water to eliminate salts. The filters were dried at 60°C for 36 to 48 h and reweighed with the microbalance. Inorganic carbon was then removed by placing the filters in a desiccator saturated with HCl fumes overnight. For particulate organic carbon (POC) and particulate nitrogen (PN) determination, samples were pelletized in tin capsules, and combustion was performed with an Elementar Pyro Elemental Analyzer, and detection with a Thermo Delta

140 XPplus Isotope Ratio Mass Spectrometer (UQAR-ISMER). Subsamples of each sample cup were also analyzed for total organic carbon (TOC) and total nitrogen (TN), allowing for the calculation of TOC:TN mass ratios, as well as the carbon (δ^{13}C) and nitrogen (δ^{15}N) isotopic signatures of the sinking particles. Each subsample was centrifuged at 3000 rpm, decanted, resuspended, and rinsed with distilled water three times. Centrifuge cycles began at 12 min and increased by 4 min intervals with each subsequent rinse. Subsamples were stored overnight at -80°C and subsequently

145 freeze-dried for 2 to 3 days. The particles were re-homogenized using an agate mortar and pestle. Subsamples used for TOC and δ^{13}C were acidified using sequential aliquots of 1 M HCl, administered in scintillation vials, until no reaction was visible. Samples were dried at 60°C before being weighed into tin capsules and loaded into a Costech 4010 Elemental Analyzer coupled to a Delta V Plus – Conflo IV Isotope Ratio Mass Spectrometer (UNB).

3.3 Chloropigments

150 Chlorophyll *a* (chl *a*) is an index of the phytoplankton biomass and can be used as an indicator of the freshness of algal inputs in sediments (Boon and Duineveld, 1996). Phaeopigments are chlorophyll degradation products resulting from cell senescence and zooplankton grazing (Mantoura and Llewellyn, 1983; Villanueva and Hastings, 2000). Thus, chloropigments (chl *a* + phaeopigments) are a reliable proxy for surface primary productivity. For chl *a* and phaeopigment measurements, subsamples of 0.25 or 0.5 mL were collected using a pipette and filtered onto 25

155 mm Whatman GF/F filters (nominal porosity of 0.7 μm). The pigments retained on the filters were extracted in 10 mL of 90% acetone for 18 to 24 h at 4°C in the dark. The supernatant was then transferred to a borosilicate tube for fluorescence measurements with a Turner Designs 10-AU fluorometer calibrated using chl *a* extract from *Anacystis*

nidulans (Sigma-Aldrich; UQAR-ISMER). Prior to phaeopigment measurements, three drops of 5% v/v HCl were added to the supernatant (Parsons et al., 1984).

160 **3.4 Phytoplankton**

For each sample, an aliquot of 80 to 150 µL was diluted with 10 mL of a preservative solution in a settling chamber and left to settle evenly over a counting chamber for a minimum of 6 h. The preservative solution consisted of 1 L of artificial seawater (30 psu) mixed with 20 mL of 37 % w/v formaldehyde. Phytoplankton were identified and counted using an inverted microscope (Olympus CKX53; UNB). A survey of the entire counting chamber was 165 first conducted at 100× magnification to identify any large phytoplankton that could be missed during the subsequent three transects at 400× magnification for the phytoplankton enumeration. Taxonomic identifications of diatoms and dinoflagellates were completed following Vinyard (1979), Hasle and Syvertsen (1997), Steidinger and Jangen (1997), Bérard-Therriault et al. (1999), and Round et al. (2007).

Daily fluxes ($m^{-2} d^{-1}$) of TPM, POC, PN, chloropigments, diatoms, and dinoflagellates were calculated based 170 on the collecting area of the trap and the sampling period, and were subsequently integrated to annual fluxes ($m^{-2} yr^{-1}$).

4 Results

4.1 Structure of the water column

During the deployment of the mooring on 15 October 2020, the euphotic zone comprised the upper 10 m, the 175 surface mixed layer extended down to 12 m, and the cold intermediate layer extended down to 65 m at the BC site (Fig. 3) At the PDM site, the euphotic zone comprised the upper 13 m, which extended below the surface mixed layer at 10 m, and a thicker cold intermediate layer extended down to 108 m. A subsurface fluorescence maximum was observed at 7 and 13.5 m at the BC site and at 5 m with a lower value at the PDM site.

At BC-133, water temperatures were highest (>5°C) in March and lowest (<1°C) in May 2021, while salinity 180 ranged from 32.0 to 34.3 psu (Fig. 4). At PDM-154, water was generally warmer, frequently reaching temperatures >5°C and never decreasing <1°C, while salinity was in the same range as at BC-133 (Fig. 5). These data confirm that all three sediment traps were located within the deep layer of the water column.
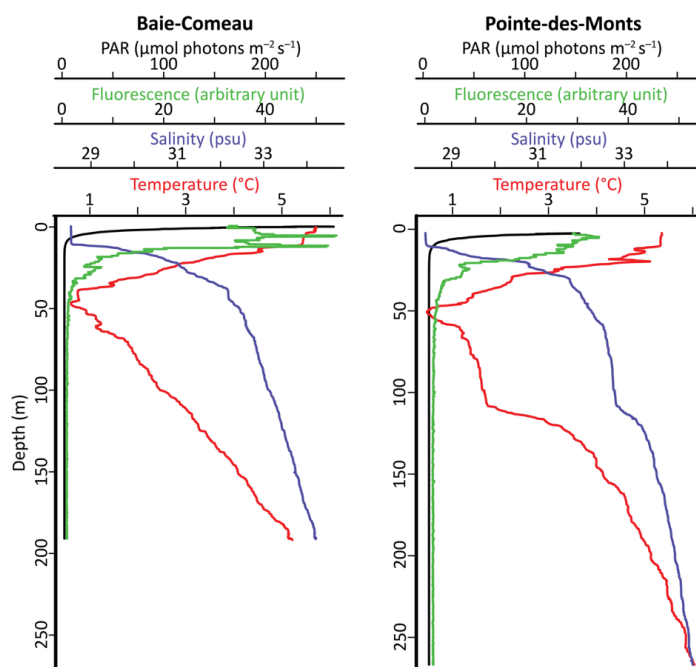
Figure 3: Vertical profiles of photosynthetically active radiation (PAR), *in vivo* **chlorophyll fluorescence, salinity, and temperature at the Baie-Comeau and Pointe-des-Monts sites on 15 October 2020.**

4.2 Magnitude and composition of particle fluxes

At BC-133, daily TPM fluxes remained lower than 1.1 g m^{-2} d^{-1} from November 2020 to September 2021 (Fig. 4). Peak chloropigment fluxes (1.6 mg m^{-2} d^{-1}) were recorded in early May 2021, concurrent with an increase in TPM, POC, and PN fluxes. Peak POC and PN fluxes were observed in early August 2021 (106.5 and 16.5 mg m^{-2} d^{-1}, respectively). Chloropigment, POC and PN fluxes remained consistently low from mid-November 2020 until April 2021. POC:PN mass ratios peaked (11.7) in February 2021, bulk sediment TOC:TN mass ratios peaked (11.3) in November 2020, δ^{13}C values peaked (-21.0 ‰) in August 2021, and δ^{15}N values peaked (9.8 ‰) in November 2020 and March 2021. Sinking particles collected at BC-133 showed relatively high POC:PN and TOC:TN mass ratios and low δ^{13}C values from November 2020 to April 2021, while the period from May to September 2021 was characterized by relatively low POC:PN and TOC:TN mass ratios and high δ^{13}C values, whereas δ^{15}N values did not reflect a seasonal trend (Fig. 4). See Appendix A for the particulate matter and chloropigment fluxes, mass ratios, and isotopic signatures at BC-133, PDM-154 and PDM-224.

At the PDM site, peak TPM fluxes occurred during the first half of February 2021 at both depths (6.5 and 7.9 g m^{-2} d^{-1} at PDM-154 and PDM-224, respectively; Fig. 5). These peak values were up to 7 times higher than the maximum value recorded at BC-133 (1.1 g m^{-2} d^{-1}; Fig. 4). Fluxes of chloropigments (1.1 mg m^{-2} d^{-1}) were highest at both PDM-154 and PDM-224 in early November 2020. Overall, fluxes of chloropigments exhibited similar patterns at both depths, with slightly higher flux values at PDM-224. Temporal variations in chloropigment and TPM fluxes were decoupled during April and May 2021 at the PDM site, contrasting with the concurrent peaks at BC-133 in early

205   May 2021. Unlike at BC-133, POC and PN fluxes were higher from November 2020 to February 2021 at both PDM-
154 and PDM-224. Peaks in POC and PN fluxes were recorded in November 2020 and February 2021 at PDM-154,
whereas values were significantly greater in November and December 2020 at PDM-224. Compared to BC-133, the
POC:PN mass ratio peaks were the same or higher (12.8 and 11.6 in PDM-154 and PDM-224, respectively) in
February 2021. TOC:TN mass ratio peaks were lower (9.5 in November 2020 at PDM-154 and 8.0 in February 2021

210   at PDM-224) than the peak measured at BC-133. δ^{13}C peak values were lower (-21.8 ‰ at PDM-154 and PDM-224)
and peaked in August 2021 while δ^{15}N peak values were higher (10.3 ‰ and 10.8 ‰ at PDM-154 and PDM-224,
respectively) and peaked in July 2021. A similar TOC:TN mass ratios against δ^{13}C pattern to BC-133 was observed
at PDM, but with less variation between the November-April and May-September periods (Fig. 6). The seasonal
pattern was less distinctive at PDM-224, where average δ^{13}C and low TOC:TN values were maintained during the

215   majority of the sampling period.
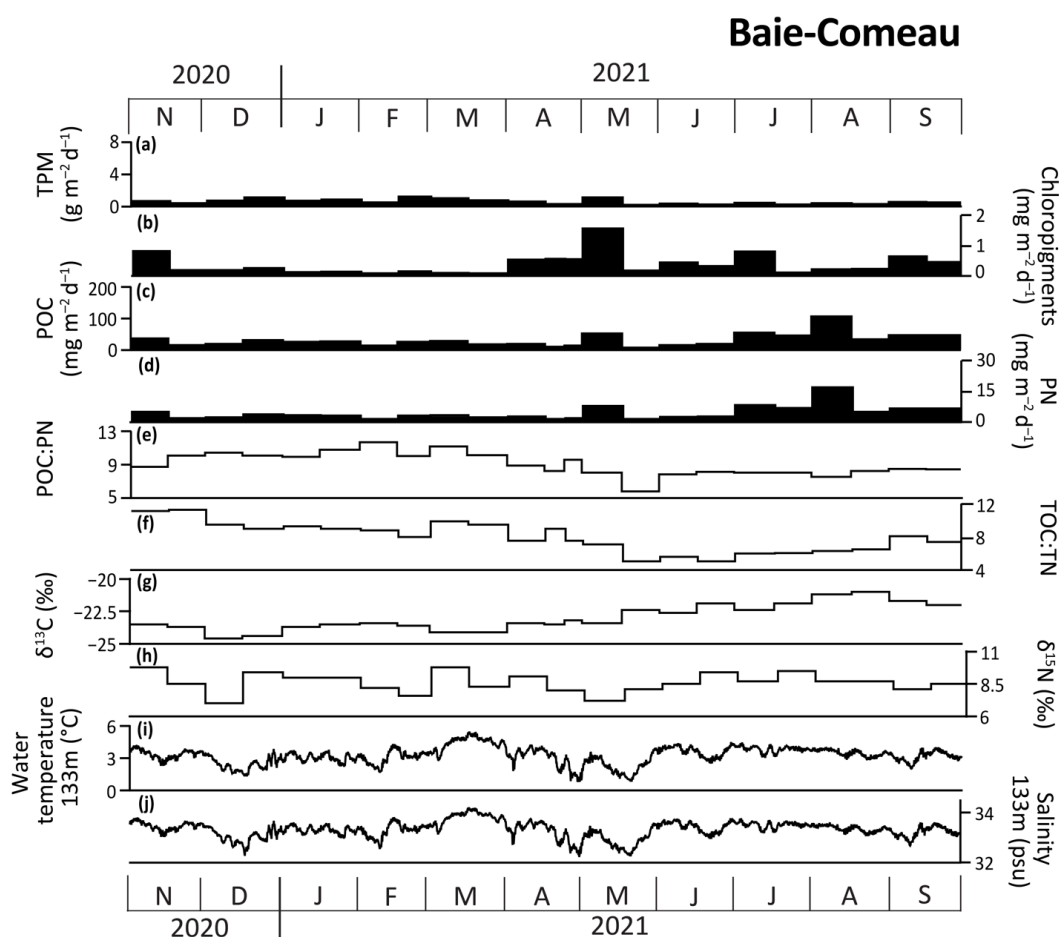
Figure 4: Data from the Baie-Comeau (BC-133) mooring site from November 2020 to September 2021. (a) Total particulate matter (TPM), (b) chloropigments, (c) particulate organic carbon (POC), and (d) particulate nitrogen (PN) fluxes, along with (e) POC:PN and (f) TOC:TN mass ratios, and (g) carbon (δ^{13}C) and (h) nitrogen (δ^{15}N) isotopic values of the sinking
220   **particles, (i) water temperature, and (j) salinity.**
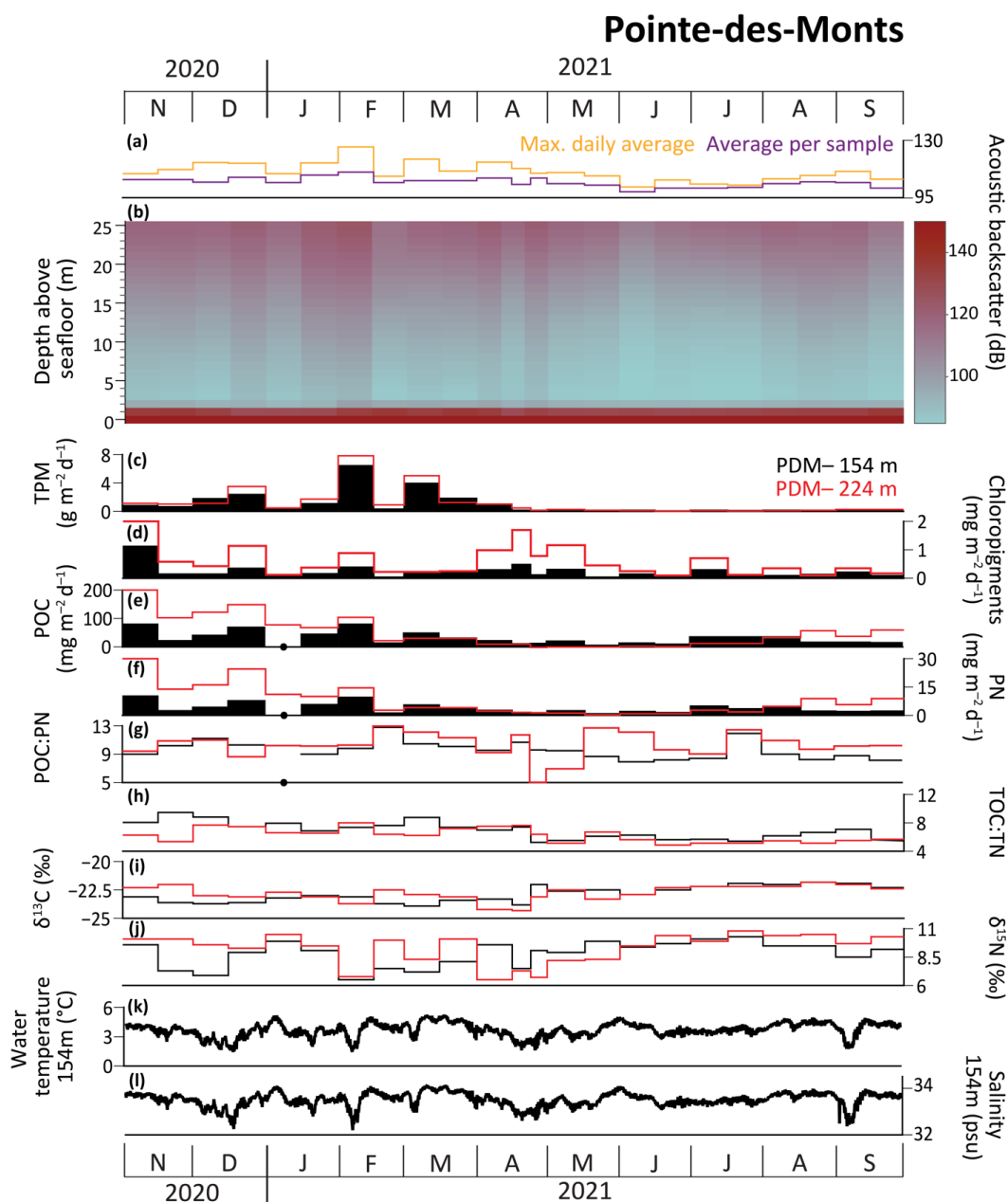
Figure 5: Data from the PDMc and PDM mooring sites from November 2020 to September 2021. a) Maximum daily average and average backscatter per sampling period and b) average backscatter per 1 m depth from ADCP, as well as c) total particulate matter (TPM), d) chloropigment, e) particulate organic carbon (POC), and f) particulate nitrogen (PN) fluxes, along with g) POC:PN and h) TOC:TN mass ratios, and i) carbon (δ^{13}C) and j) nitrogen (δ^{15}N) isotopic values of the sinking particles, k) water temperature, and l) salinity. Black dots indicate that there is no POC or PN data for PDM-154 for early January 2021.

225
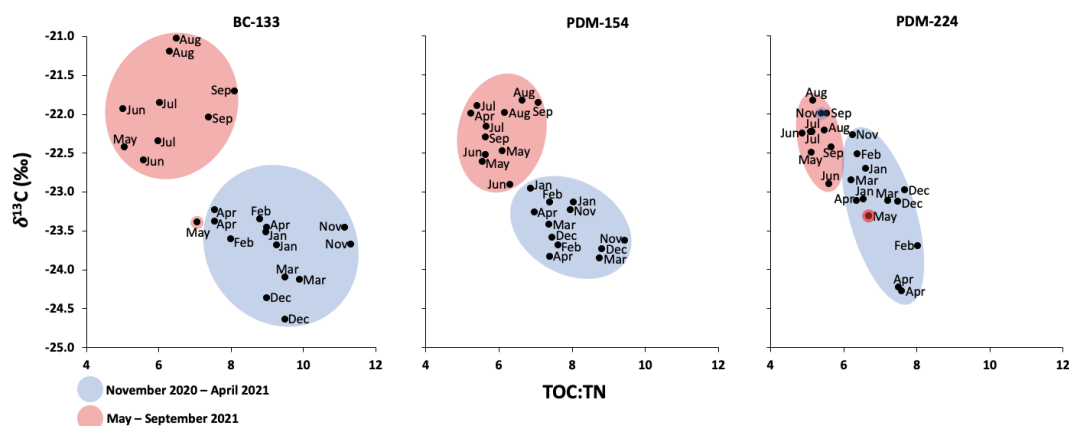
Figure 6: Carbon isotopic values against TOC:TN mass ratios of sinking particles collected at the Baie-Comeau and Pointe-des-Monts sites from November 2020 to September 2021. The two samples for the month of May, highlighted in pink, are distinct in BC-133 and PDM-224.

230

4.3 Magnitude and composition of phytoplankton fluxes

At BC-133, diatom fluxes were 2 orders of magnitude higher than dinoflagellate fluxes (Fig. 7 and 8). Fluxes of centric diatoms were always higher than pennate diatoms, except during late September 2021, when fluxes of the potentially harmful pennate diatom *Pseudo-nitzschia seriata* were elevated (Fig. 7). In accordance with chloropigment fluxes, peaks in diatom ($\sim 87 \times 10^6$ frustules m^{-2} d^{-1}), dinoflagellate theca ($\sim 14 \times 10^4$ thecae m^{-2} d^{-1}) and dinoflagellate cyst ($\sim 9 \times 10^4$ cysts m^{-2} d^{-1}) fluxes were observed in early May 2021. The pennate diatom *Pseudo-nitzschia* spp. and the centric diatoms *Chaetoceros* spp., *Skeletonema* spp., and *Thalassiosira* spp. dominated the diatom assemblages. Relative contributions of dinoflagellate thecae and cysts varied throughout the year, with a large contribution of the genus *Protoperidinium* spp. ($\sim 14 \times 10^6$ thecae m^{-2} d^{-1}) in early May (Fig. 8). *Dinophysis acuminata* and *D. norvegica,* two dinoflagellate species known for producing okadaic acid group toxins associated with Diarrhetic Shellfish Poisoning (Bates et al., 2020), were observed in June and August 2021 at BC-133. See Appendix B for the complete list of diatom and dinoflagellate taxa observed and photo plates showing representative specimens.

At PDM-154, the peak in diatom fluxes ($\sim 73 \times 10^6$ frustules m^{-2} d^{-1}) was observed in mid-April 2021, while the peak in dinoflagellate fluxes ($\sim 15 \times 10^4$ thecae m^{-2} d^{-1}) occurred in early July 2021 (Fig. 7 and 8). From December 2020 to early April 2021, pennate diatom fluxes were often similar or higher than centric diatom fluxes, while centric taxa dominated the diatom fluxes during November 2020 and from late April to September 2021. All the dominant diatom taxa showed lower fluxes at PDM-154 compared to BC-133 (Fig. 7) and none of the maximum fluxes for the dominant diatoms were synchronous between the two sites. At PDM-154, dinoflagellates were rarely collected before May 2021, apart from *Dinophysis* spp., which were present in early December 2020. However, we note that the dinoflagellate cyst *Brigantedinium* spp. was observed in December, February, and March 2021.
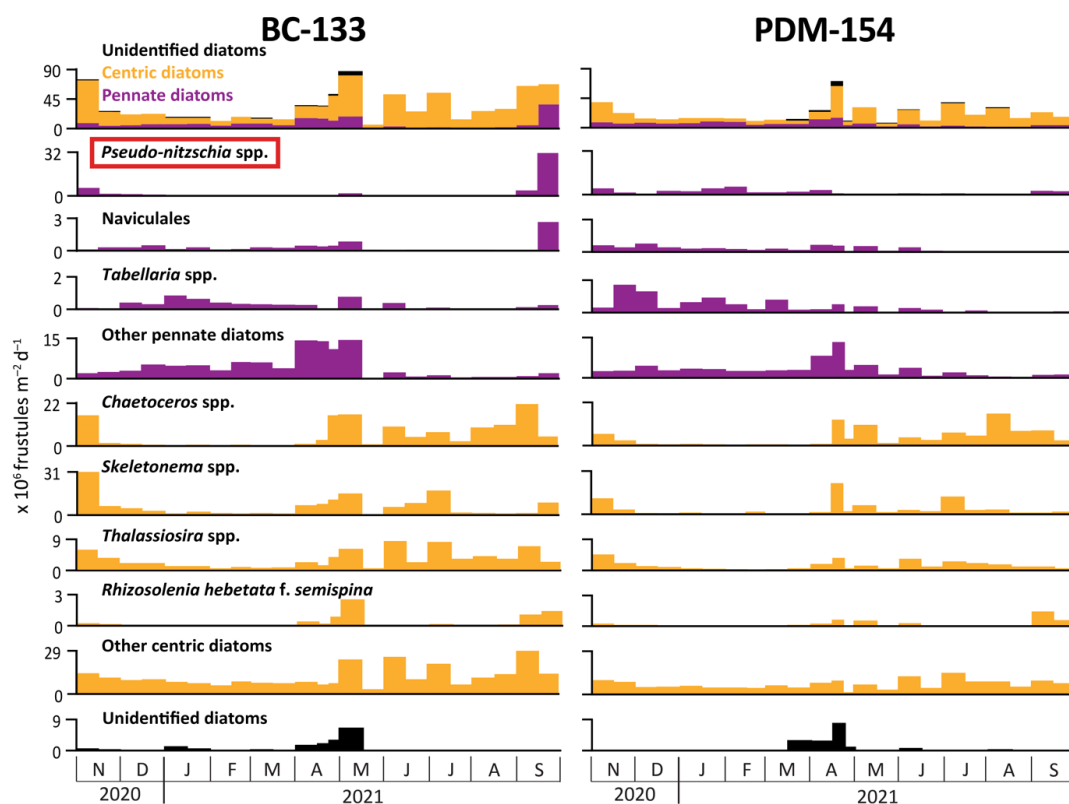
Figure 7: Fluxes of dominant diatoms measured at Baie-Comeau (BC-133) and Pointe-des-Monts (PDM-154) from November 2020 to September 2021. The top panel indicates total diatom fluxes, distinguishing unidentified, centric, and pennate diatom groupings. The red box indicates a potentially harmful taxon. Several genera were grouped together in the order Naviculales (*Diploneis* spp., *Gyrosigma/Pleurosigma* spp., *Navicula* spp., and cf. *Plagiotropis* spp.).

255
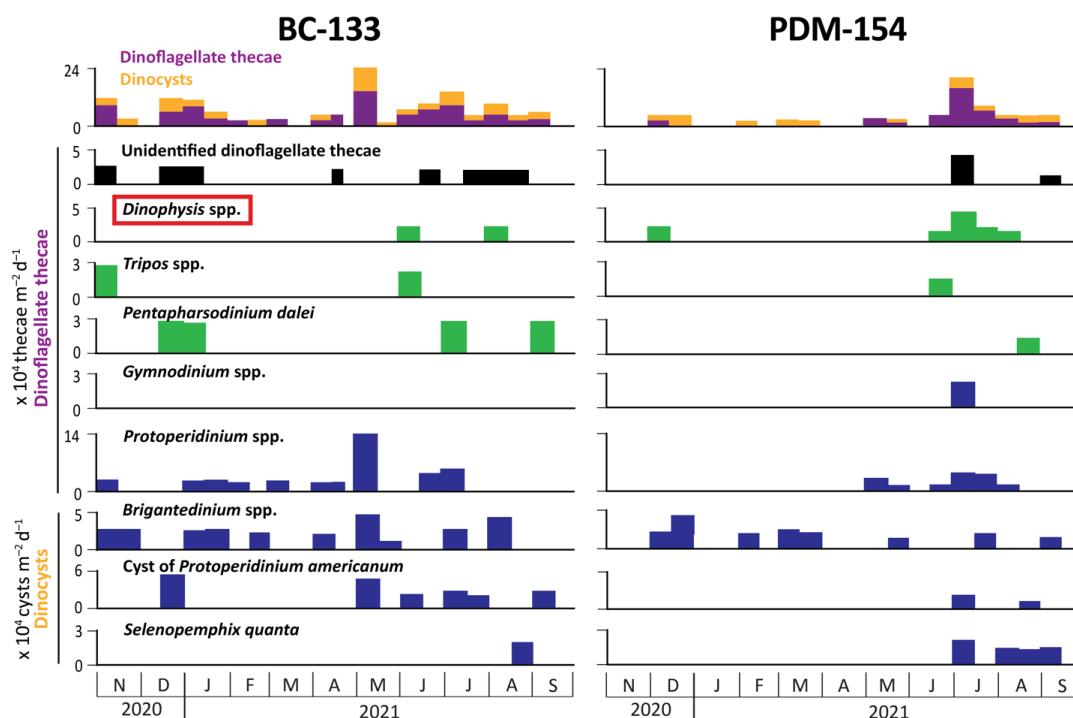
Figure 8: Fluxes of dinoflagellate thecae and dinoflagellate cysts (dinocysts) measured at Baie-Comeau (BC-133) and Pointe-des-Monts (PDM-154) from November 2020 to September 2021. The top panel indicates total dinoflagellate fluxes, distinguishing thecae and cysts. The red box indicates a potentially harmful taxon. Green indicates autotrophic taxa and blue indicates heterotrophic taxa.

4.4 Annual fluxes

Annual fluxes of chloropigments, diatoms, and dinoflagellates were almost 2 times higher at BC-133 than at PDM-154 (Table 2). In contrast, annual fluxes of TPM, POC, and PN were highest at PDM-224, where the TPM flux value was more than 2 times higher than at BC-133.

Table 2: Annual fluxes measured at the Baie-Comeau (BC-133) and Pointe-des-Monts (PDM-154 and PDM-224) sites from November 2020 to September 2021. N/A: not available.

	BC-133	PDM-154	PDM-224
TPM (g m^{-2} yr^{-1})	168	354	429
POC (g m^{-2} yr^{-1})	11	11	19
PN (g m^{-2} yr^{-1})	1.5	1.3	2.5
Chloropigments (mg m^{-2} yr^{-1})	120	70	92
Diatoms ($\times 10^9$ frustules m^{-2} yr^{-1})	11	6.8	N/A
Dinoflagellates ($\times 10^6$ thecae+cysts m^{-2} yr^{-1})	20	11.1	N/A

4.5 Backscatter data in the main Pointe-des-Monts canyon

The average backscatter measured at PDMc ranged from 98.7 to 110.8 dB, with a peak during the first half
of February 2021 (Fig. 5a). This peak was associated with a small turbidity current that occurred on 3 February 2021
(Appendix C, Fig. C1). The maximum daily average of backscatter for each trap sampling period ranged from 101.7
to 126.2 dB, with the highest value recorded concurrently with enhanced TPM and POC at both PDM-154 and PDM-
224 (Fig. 5a, c, e). A smaller resuspension event was identified on 22–23 December 2020 based on a sharp increase
of backscatter near the seafloor (Fig. 5b), which also occurred concurrently with enhanced TPM and POC fluxes. TPM
fluxes at both depths were positively correlated with the average backscatter ($R^2 = 0.456$ for PDM-154 and 0.586 for
PDM-224; $p < 0.01$) and maximum daily average backscatter ($R^2 = 0.652$ for PDM-154 and 0.751 for PDM-224; $p <$
0.001).

5 Discussion

5.1 Canyon-related sediment resuspension events

Normandeau et al. (2020) determined that turbidity currents in the PDM canyon system are associated with
sustained windstorms that create large waves which remobilize sediment on the shelf at low tide. Based on repeat
bathymetric data, they estimated that the upper region of the main canyon, the most active part of the system,
experiences a minimum of one turbidity current every 2–3 years that is large enough to cause migration of crescentic
bedforms in the canyon. However, recent ultra-high-resolution surveys suggest that smaller turbidity currents are
likely occurring more frequently but are not strong enough to erode the seafloor and are thus not observed through
bathymetric data alone (Normandeau et al., 2022). Continuous measurements of the hydrodynamics in the main axis
of the canyon during the present study identified one small turbidity current on 3 February 2021 based on a
combination of high backscatter values and a sharp increase in down-canyon water velocity. This event concurred
with the highest daily wind gusts recorded for that year (>90 km h^{-1}; Government of Canada Past Weather and Climate
Historical Data). Increased backscatter (i.e., sediment resuspension) from complex hydrodynamic processes (e.g.,
turbidity currents, upwelling and downwelling currents, internal tides, internal waves) in the main canyon was
associated with increased TPM fluxes at both PDM-154 and PDM-224. The small turbidity current event on 3
February 2021 showed some lofting (i.e., heavy sediments sink but lighter sediments rise in the water column), which
may have been sustained by a strong pycnocline (Fig. 9). Thus, we propose that the vertical structure of the water
column may have contributed to enhancing lateral dispersion of resuspended sediments, which may enhance the
regional impact of canyon sediment processes. Our data suggest that despite the relatively small size of the PDM
canyon system and relative weakness of the recorded turbidity current, it nonetheless influenced the vertical fluxes of
particles at a lateral distance of >2.6 km within the deep water-column layer. This is supported by the annual TPM
flux being more than 2 times higher at PDM-154 than BC-133, with the maximum daily TPM flux being 6 times
higher during early February 2021. Thus, our data suggest that larger turbidity currents, which are estimated to occur
every 2–3 years (Normandeau et al., 2020), may have relatively severe and wide-spread impacts on the PDM region.

A smaller resuspension event was identified on 22–23 December 2020 based on a sharp increase of backscatter near the seafloor but lacked the sharp increase in down-canyon water velocity required of a turbidity current. This event was not correlated with significant wind gusts (<33 km h⁻¹; Government of Canada Past Weather and Climate Historical Data). During this smaller resuspension event, TPM fluxes increased at the PDM site, albeit values were lower than those associated with the turbidity current.
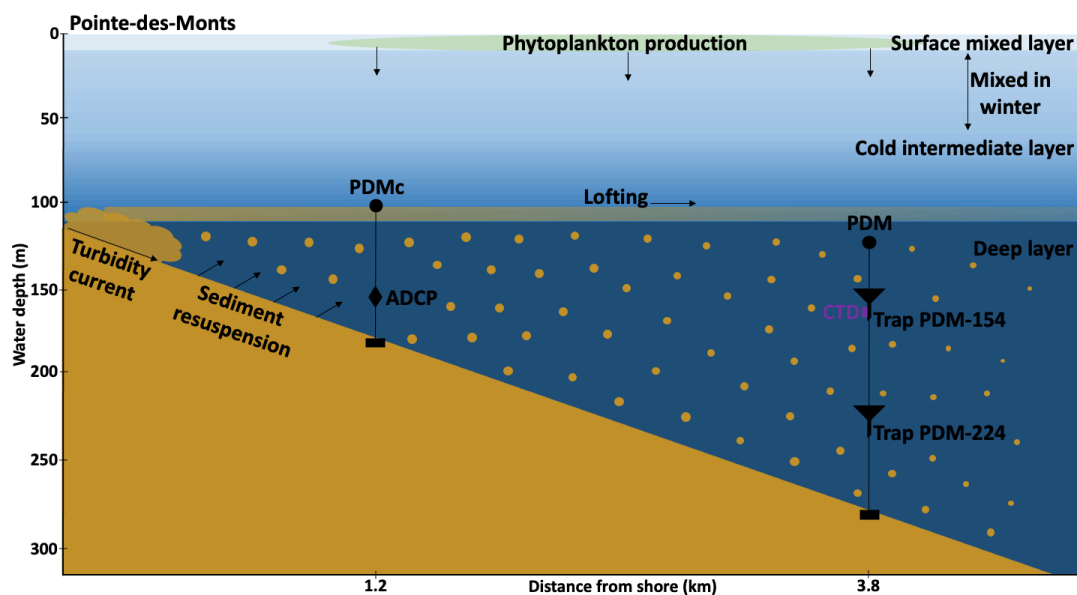
Figure 9: Schematic showing a turbidity current event with sediment resuspension and lofting contributing to increased biogenic matter in the sediment traps.

POC:PN ratios are used as an indicator of nutrient limitation or relative diagenetic state (i.e., "chemical freshness") of marine particulate organic matter, with values around 6 to 8 being representative of labile organic matter, and degraded organic matter typically yielding values >10 (e.g., Redfield, 1958; Walker et al., 2016; Fox and Walker, 2022). In the present study, the highest POC:PN mass ratio value (12.8), recorded at PDM-154 m during the second half of February 2021, likely indicates increased contributions of comparatively more degraded particulate matter resulting from resuspension of relatively older material from the seafloor. Additionally, enhanced POC and PN fluxes observed during both remobilization events were concurrent with small increases in the chloropigment fluxes, which were mostly comprised of degradation-indicative phaeopigments. Thus, we infer that canyon-related resuspension events had an impact on biogeochemical cycling in the deep layer, remobilizing and advecting particulate organic matter in the water column during winter when supplies to benthic communities are typically limited.

5.2 Sources of biogenic matter

Discrimination between autochthonous and allochthonous contributions to organic matter can be done using POC:PN mass ratios and bulk sediment δ^{13}C signatures. Marine sources are typically characterized by POC:PN mass ratios of 4 to 10 and δ^{13}C of -20 to -24 ‰, while terrestrial sources have POC:PN mass ratios of 20 to 100 and a δ^{13}C

signature around -27 ‰ because the majority of photosynthetic plants found along the coasts of the LSLE produces

330   organic matter using a C_3 Calvin pathway Meyers, 1994; Macdonald et al., 2004). In the present study, POC:PN mass

ratios (5.1 to 12.8) and measured $\delta^{13}C$ values (-24.6 to -21.0 ‰), indicate that the sinking particles collected at both

sites were of predominantly marine origin with some terrestrial influence. Sinking particles collected at BC-133 were

likely influenced by the Manicouagan River, which transports terrestrial material into the estuary (Therriault and

Levasseur, 1985). The terrestrial influence appeared relatively higher from November 2020 to April 2021 at BC-133,

335   as indicated by high bulk sediment TOC:TN mass ratios and low $\delta^{13}C$ values (Fig. 6), as well as high POC:PN mass

ratios. This is likely due to the four hydroelectric dams located in the Manicouagan River, which retain large reservoirs

of water from the spring runoff and then release during the fall and winter when electricity demands increase (Lavoie

et al., 2017). By contrast, the PDM site does not receive inputs of matter from a local freshwater system, but instead

from resuspended sediments from the seafloor (e.g., Normandeau et al., 2020).

340   Bulk sediment $\delta^{15}N$ provides valuable information regarding nutrient sources, nitrogen utilization, and trophic

alteration. Phytoplankton selectively uptake and assimilate light nitrate ($^{14}NO_3^-$), or ammonia ($^{14}NH_3$) when available,

and must incorporate increasingly more $^{15}NO_3^-$ as nitrogen concentrations become depleted in surface waters (Altabet

and Francois, 1994; Waser et al., 1998; Altabet and Francois, 2001 and references therein; Minagwa et al., 2001).

Thus, the $\delta^{15}N$ signature of sinking particles collected in the traps would be expected to increase during and following

345   the main bloom period (Wada and Hattori, 1978; Altabet et al., 1991; Nakatsuka et al., 1992; Sigman et al., 1999;

Altabet and Francois, 2001). In both PDM traps, we observed variable $\delta^{15}N$ values until the spring bloom in April

2021, followed by high values until September 2021, but we note no correlation to other primary production proxies.

This may be because the bulk samples contained all nitrogen forms, including nitrogen-bearing lithics (Kienast et al.,

2005) and organic matter sorbed onto resuspended fine clays and silts (Mayer, 1994) which undergo selective removal

350   of nitrogen-containing compounds during degradation and early diagenesis (Close, 2019). This is particularly relevant

for sinking particles collected at the BC and PDM sites, where PN fluxes comprise only a small proportion (<1%) of

the TPM fluxes. We therefore propose that bulk $\delta^{15}N$ analysis of the organic-only fraction would be more informative

for studies along the north shore of the LSLE.

5.3 Phytoplankton dynamics

355   At both BC-133 and PDM-154, relatively high diatom fluxes were sustained for seven months, during

November 2020 and from April to September 2021, exhibiting a long production season for the region (Therriault and

Levasseur, 1985; Blais et al., 2021; Genin et al., 2021). Diatom fluxes were unusually high during November 2020,

particularly at BC-133, which may be attributed to riverine and coastal nutrient input. Importantly, the 2020-2021

winter season experienced anomalous nearly ice-free conditions with above-average sea-surface temperatures

360   delaying sea ice formation (Galbraith et al., 2022), which may have played a key role in the elevated diatom fluxes in

November 2020. The predicted climate-induced decline in sea ice cover will likely have important implications on

primary production, including a lengthening of the production season. In addition, reduced sea ice cover exposes the

coastal area near PDM to increased potential for sediment remobilization events during winter (Ruest et al., 2016),

highlighting the necessity of understanding how these events influence regional primary production. Thus, in the

365   context of climate warming, this study provides valuable insight into future trends in the LSLE, which could have impacts on regional ecosystems. We note that since the present study covers an anomalous period in terms of sea ice, we cannot definitively determine if the long diatom production season observed here was typical of the study sites, or if it was lengthened due to nearly ice-free winter conditions. Thus, we recommend continued monitoring to gather more information in consecutive years under a wider range of environmental conditions.

370   Primary producer assemblages in the LSLE have been reported to be dominated by pennate diatoms in the spring and centric diatoms in the early summer, followed by dinoflagellates (Levasseur et al., 1984; Therriault and Levasseur, 1985; Roy et al., 1996; Romero et al., 2000). Here, diatom fluxes suggest that the spring diatom bloom occurred earlier at PDM-154 (mid-April 2021) than at BC-133 (early May 2021). Both sites displayed several subsequent peaks throughout the summer and fall months, but those observed at BC-133 were notably of higher

375 magnitude (Fig. 7). The similar compositional assemblages but distinct magnitude and timing of diatom fluxes at the two sites likely reflect differential nutrient inputs. One could hypothesize that canyon-related hydrodynamics would stimulate phytoplankton production at the PDM site because past studies have shown that the complex hydrodynamics of large submarine canyons increase the occurrence of biodiversity hotspots (Fernandez-Arcaya et al., 2017 and references therein; Paull et al., 2018; Santora et al., 2018). However, phytoplankton fluxes do not provide evidence

380 that this applies at PDM, a relatively small and shallow submarine canyon system. Instead, annual fluxes of diatoms and dinoflagellates were lower at PDM-154 compared to BC-133. At the PDM site, in addition to the absence of direct riverine input and differences in the structure of the water column, increased sediment input from the coast and seafloor remobilization by canyon processes may have hindered primary production by limiting light availability. As seen with the small turbidity current on 3 February 2021, a strong pycnocline between the cold intermediate layer and the deep

385 layer can enhance sediment lofting and allow resuspended sediments to stay in the water column for a longer time and over a larger region, before settling on the seafloor. However, our data do not permit to evaluate if lofted sediments also reached the surface layer where they would have directly impacted primary production. Additionally, we observed lower phytoplankton fluxes at PDM-154 throughout the annual cycle, but from our dataset, we cannot evaluate if sediment lofting would play a key role in this system throughout the entire year, or only during turbidity currents and

390 other sediment remobilization events, which appear to be more frequent during the fall and winter.

5.4 Potentially harmful phytoplankton taxa

    At BC-133, large fluxes of the pennate diatom *Pseudo-nitzschia seriata* were observed (~ 32×10^6 frustules m^{-2} d^{-1}) during the second half of September 2021, suggesting the occurrence of an autumn bloom. This species produces domoic acid associated with Amnesic Shellfish Poisoning, which has led to mortality of humans, marine

395 mammals, fish, and birds worldwide, but has not yet been fatal in Canadian waters (Bates et al., 2020 and references therein). No concerning ecological effects were reported at that time (e.g., high toxin levels, mortalities) and the bloom was relatively constrained spatially as it was not observed as far east as PDM-154. Concentrations greater than 5,000 cells L^{-1} of *P. seriata* are generally considered harmful algal blooms, although toxin production is variable and is not always correlated to cell abundance, but rather dependent on several factors such as salinity, temperature, pH, and

400 nutrient limitations (Boivin-Rioux et al., 2022 and references therein). The dinoflagellates *Dinophysis acuminata* and

D. norvegica, which produce okadaic acid group toxins associated with Diarrhetic Shellfish Poisoning, a non-deadly but severe gastrointestinal illness, were also present in low abundances in sinking particles collected at both sites. Our data do not show evidence of the potential role of canyon processes for the inoculation of harmful algal blooms in the water column during the 2020–2021 deployment period. However, a more detailed analysis focused on harmful algae
405 would be required to quantify this relationship.

5.5 Flux comparison with previous sediment trap studies

TPM fluxes previously measured in the LSLE during May and July (1.8 to 11.3 g m^{-2} d^{-1}; 150 m trap depth, 350 m bottom depth; Colombo et al., 1996), were much higher than those measured in this study for the same spring and summer months (0.1 to 1.0 g m^{-2} d^{-1}). However, total mass fluxes from an annual cycle in the Gulf of Maine
410 (max. 0.12 g m^{-2} d^{-1} in May; 150 m trap depth, 280 m water depth; Pilskaln et al., 2014) and from several drifting sediment trap deployments in the Gulf of St. Lawrence (max. 1.6 g m^{-2} d^{-1} in June; 50 and 150 m trap depths; Romero et al., 2000) were significantly lower than TPM fluxes measured at both sites in our study. Annual chloropigment and POC fluxes measured here were much greater than those measured near Cabot Strait (35.9 mg m^{-2} yr^{-1} and 1.1 g m^{-2} yr^{-1}, respectively; Genin et al., 2021), suggesting enhanced biological productivity in the estuarine system compared
415 to the seaward entrance of the Gulf of St. Lawrence. These variations in flux measurements could be attributed to many factors including variations in environmental conditions, local productivity, sediment trap deployment and laboratory methods.

6 Conclusion

Time-series biogenic matter fluxes and ADCP data indicate that the PDM submarine canyon system
420 experienced a minor sediment remobilization event on 22–23 December 2020 and a small turbidity current on 3 February 2021. Both events led to enhanced particle fluxes over the submarine fan >2.6 km further offshore. We suggest that larger turbidity currents, which are estimated to occur every 2–3 years, potentially have wide-spread impacts on fluxes of biogenic matter in the PDM region. The events recorded here influenced biogeochemical cycling in the deep layer by remobilizing and advecting biogenic matter, as reflected by concurrent elevated POC, PN, and
425 chloropigment fluxes. Sinking particles collected at the base of the submarine canyon (PDM-154) and outside the canyon system (BC-133) had similar compositional assemblages of diatoms and dinoflagellates. However, our data show that annual phytoplankton fluxes were lower in the canyon compared with background LSLE values as recorded at Baie-Comeau. We also show that the potentially harmful pennate diatom *Pseudo-nitzschia seriata* and dinoflagellates *Dinophysis acuminata* and *D. norvegica* were present at both sites. The 2020–2021 winter season
430 experienced anomalous nearly ice-free conditions, which may have implications on the length of the diatom production season and likelihood of remobilization events in the PDM canyon. Thus, in the context of climate warming, this study provides valuable insight into future trends of biogenic matter export in the LSLE, which could have regional ecological impacts. We thereby recommend continued monitoring of the canyons, using ADCPs and sediment traps, to gather more information in consecutive years under a wider range of environmental conditions.

Appendix A

Table A1: Total particulate matter flux (TPM), chlorophyll *a* flux (chl *a*), phaeopigment flux (phaeo), chloropigment flux (chl *a* + phaeo), particulate organic carbon flux (POC), particulate nitrogen flux (PN), POC:PN mass ratio, TOC:TN mass ratio, carbon (δ^{13}C), and nitrogen (δ^{15}N) isotopic values at the Baie-Comeau mooring site (BC-133) from November 2020 to September 2021.

Start	TPM	Chl *a*	Phaeo	Chloropigments	POC	PN	POC:PN	TOC:TN	δ^{13}C	δ^{15}N
d/m/yr	g m^{-2} d^{-1}			mg m^{-2} d^{-1}			g:g		‰	
31/10/20	0.5	0.08	0.74	0.81	35.6	4.8	8.8	11.2	-23.5	9.8
15/11/20	0.3	0.01	0.16	0.17	14.3	1.7	10.1	11.3	-23.7	8.5
30/11/20	0.6	0.02	0.15	0.17	17.7	2.0	10.4	9.5	-24.6	7.0
15/12/20	1.0	0.03	0.21	0.24	30.1	3.5	10.1	9.0	-24.4	9.4
31/12/20	0.6	0.01	0.08	0.09	25.2	3.0	10.0	9.3	-23.7	9.0
15/01/21	0.7	0.01	0.10	0.12	26.1	2.9	10.8	9.0	-23.5	9.0
31/01/21	0.4	0.01	0.05	0.05	13.1	1.3	11.7	8.8	-23.4	8.2
15/02/21	1.1	0.01	0.11	0.12	25.3	2.9	10.1	8.0	-23.6	7.6
28/02/21	0.9	0.01	0.06	0.07	27.6	3.0	11.2	9.9	-24.1	9.8
15/03/21	0.6	0.01	0.06	0.06	17.1	2.0	10.1	9.5	-24.1	8.3
31/03/21	0.5	0.06	0.48	0.53	18.2	2.4	8.9	7.6	-23.4	9.1
15/04/21	0.2	0.03	0.53	0.56	8.7	1.2	8.3	9.0	-23.5	8.0
23/04/21	0.2	0.05	0.49	0.54	13.3	1.6	9.6	7.6	-23.2	8.0
30/04/21	1.0	0.13	1.45	1.58	52.3	7.6	8.1	7.1	-23.4	7.2
16/05/21	0.1	0.01	0.15	0.16	5.8	1.2	5.8	5.1	-22.4	8.1
31/05/21	0.2	0.04	0.40	0.44	14.6	2.2	7.9	5.6	-22.6	8.5
15/06/21	0.2	0.02	0.28	0.30	17.5	2.5	8.2	5.0	-21.9	9.4
30/06/21	0.4	0.09	0.71	0.80	54.6	8.0	8.0	6.0	-22.4	8.7
16/07/21	0.2	0.01	0.08	0.09	45.1	6.6	8.0	6.0	-21.9	9.5
31/07/21	0.3	0.02	0.18	0.20	106.5	16.5	7.5	6.3	-21.2	8.7
16/08/21	0.2	0.02	0.19	0.21	33.4	4.8	8.2	6.5	-21.0	8.7
31/08/21	0.4	0.07	0.56	0.63	46.0	6.3	8.5	8.1	-21.7	8.1
15/09/21	0.4	0.08	0.37	0.44	45.9	6.4	8.5	7.4	-22.0	8.5

450

Table A2: Total particulate matter flux (TPM), chlorophyll *a* flux (chl *a*), phaeopigment flux (phaeo), chloropigment flux (chl *a* + phaeo), particulate organic carbon flux (POC), particulate nitrogen flux (PN), POC:PN mass ratio, TOC:TN mass ratio, carbon (δ^{13}C), and nitrogen (δ^{15}N) isotopic values at the upper Pointe-des-Monts mooring site (PDM-154) from November 2020 to September 2021. N/A = not available.

Start	TPM	Chl *a*	Phaeo	Chloropigments	POC	PN	POC:PN	TOC:TN	δ^{13}C	δ^{15}N
d/m/yr	g m^{-2} d^{-1}			mg m^{-2} d^{-1}				g:g		‰
31/10/20	0.8	0.04	1.08	1.12	79.8	10.1	9.0	8.1	-23.1	9.6
15/11/20	0.7	0.01	0.14	0.15	21.8	2.5	10.2	9.5	-23.6	7.3
30/11/20	1.8	0.01	0.14	0.15	40.9	4.2	11.3	8.8	-23.7	6.9
15/12/20	2.4	0.03	0.31	0.34	68.5	7.7	10.3	7.5	-23.6	8.9
31/12/20	0.4	0.00	0.06	0.06	N/A	N/A	N/A	8.0	-23.2	9.9
15/01/21	1.1	0.01	0.14	0.15	44.3	5.8	9.0	6.9	-23.0	9.1
31/01/21	6.5	0.05	0.34	0.39	79.9	9.5	9.8	7.4	-23.1	6.5
15/02/21	0.4	0.01	0.03	0.04	13.2	1.2	12.8	7.6	-23.7	7.5
28/02/21	4.0	0.03	0.19	0.22	49.0	5.5	10.5	8.8	-23.9	7.2
15/03/21	1.9	0.03	0.20	0.23	31.5	3.6	10.1	7.4	-23.4	8.1
31/03/21	1.0	0.03	0.26	0.29	21.9	2.7	9.6	7.0	-23.3	9.6
15/04/21	0.2	0.06	0.43	0.49	10.4	1.2	10.7	7.4	-23.8	7.5
23/04/21	0.1	0.01	0.11	0.12	12.1	1.5	9.6	5.3	-22.0	9.1
30/04/21	0.2	0.03	0.28	0.31	20.3	2.5	9.5	5.6	-22.6	8.9
16/05/21	0.1	0.00	0.03	0.04	5.6	0.8	8.7	6.1	-22.5	9.9
31/05/21	0.2	0.01	0.13	0.14	13.1	1.9	7.9	6.3	-22.9	9.4
15/06/21	0.1	0.00	0.03	0.03	9.8	1.4	8.2	5.6	-22.5	9.7
30/06/21	0.2	0.03	0.26	0.29	34.6	4.8	8.4	5.7	-22.2	10.1
16/07/21	0.1	0.01	0.07	0.08	34.9	3.4	12.0	5.4	-21.9	10.3
31/07/21	0.2	0.01	0.08	0.09	35.2	4.6	9.0	6.2	-22.0	9.5
16/08/21	0.1	0.01	0.12	0.13	15.9	2.3	8.3	6.7	-21.8	9.5
31/08/21	0.2	0.02	0.19	0.21	15.6	2.1	8.8	7.1	-21.9	8.5
15/09/21	0.2	0.01	0.08	0.09	15.1	2.2	8.2	5.7	-22.3	9.2

455

460

465 **Table A3: Total particulate matter flux (TPM), chlorophyll *a* flux (chl *a*), phaeopigment flux (phaeo), chloropigment flux (chl *a* + phaeo), particulate organic carbon flux (POC), particulate nitrogen flux (PN), POC:PN mass ratio, TOC:TN mass ratio, carbon (δ^{13}C), and nitrogen (δ^{15}N) isotopic values at the lower Pointe-des-Monts mooring site (PDM-224) from November 2020 to September 2021.**

Start	TPM	Chl *a*	Phaeo	Chloropigments	POC	PN	POC:PN	TOC:TN	δ^{13}C	δ^{15}N
d/m/yr	g m^{-2} d^{-}			mg m^{-2} d^{-1}			g:g		‰	
31/10/20	1.2	0.10	0.95	1.05	203.8	27.5	8.7	6.3	-22.3	10.1
15/11/20	1.1	0.03	0.26	0.29	109.1	12.9	9.9	5.4	-22.0	10.1
30/11/20	1.1	0.02	0.19	0.21	127.8	15.0	10.0	7.7	-23.0	9.6
15/12/20	3.6	0.06	0.54	0.60	153.9	22.4	8.0	7.5	-23.1	9.3
31/12/20	0.5	0.01	0.05	0.05	84.8	10.6	9.3	6.6	-22.7	10.5
15/01/21	1.7	0.02	0.16	0.18	76.0	9.5	9.3	6.6	-23.1	9.5
31/01/21	7.9	0.07	0.38	0.45	110.5	13.7	9.4	8.0	-23.7	6.8
15/02/21	0.9	0.01	0.09	0.10	31.3	3.2	11.6	6.4	-22.5	10.0
28/02/21	5.1	0.01	0.09	0.10	39.5	4.2	10.9	6.2	-22.9	8.3
15/03/21	1.2	0.02	0.10	0.12	38.9	4.3	10.2	7.2	-23.1	10.1
31/03/21	1.0	0.05	0.46	0.51	19.2	2.7	8.5	7.5	-24.2	6.5
15/04/21	0.5	0.07	0.83	0.90	18.2	2.0	10.6	7.6	-24.3	7.3
23/04/21	0.2	0.05	0.35	0.40	7.8	1.8	5.1	6.4	-23.1	6.7
30/04/21	0.3	0.07	0.53	0.60	8.8	1.6	6.7	5.1	-22.5	8.2
16/05/21	0.2	0.01	0.21	0.22	8.7	0.9	11.4	6.7	-23.3	8.3
31/05/21	0.1	0.01	0.11	0.12	12.6	1.4	10.9	5.6	-22.9	9.5
15/06/21	0.0	0.01	0.03	0.04	10.1	1.3	8.9	4.9	-22.3	10.4
30/06/21	0.1	0.05	0.32	0.37	22.0	3.1	8.4	5.1	-22.2	9.9
16/07/21	0.1	0.01	0.05	0.05	20.9	2.3	11.2	5.1	-22.2	10.8
31/07/21	0.1	0.01	0.15	0.16	42.1	5.0	10.0	5.5	-22.2	10.4
16/08/21	0.2	0.00	0.03	0.03	64.7	8.5	8.9	5.2	-21.8	10.5
31/08/21	0.3	0.01	0.16	0.17	45.8	5.8	9.3	5.6	-22.0	9.7
15/09/21	0.3	0.01	0.06	0.07	67.4	8.5	9.3	5.7	-22.4	10.3

470

Appendix B

475 **Table B1: Diatom taxa identified in the moored sediment traps at Baie-Comeau (BC-133) and Pointe-des-Monts (PDM-154). P = present in study site.**

		BC-133	**PDM-154**
Centric diatoms	*Chaetoceros* spp.	P	P
	Corethron hystrix	P	P
	Coscinodiscus radiatus	P	P
	cf. *Dactyliosolen fragilissimus*	P	-
	Detonula confervacea	P	P
	Eucampia groenlandica	P	P
	Eupyxidicula turris	P	P
	Melosira spp.	P	-
	Odontella aurita	P	P
	Paralia sulcata	P	-
	cf. *Porosira glacialis*	P	P
	Proboscia eumorpha	P	P
	Rhizosolenia hebetata f. *semispina*	P	P
	Skeletonema spp.	P	P
	Thalassiosira spp.	P	P
Pennate diatoms	cf. *Amphora* spp.	P	P
	Asterionella spp.	P	P
	Cocconeis spp.	P	P
	Diploneis spp.	P	-
	Entomoneis spp.	P	P
	cf. *Epithemia* spp.	P	-
	Fragilariopsis oceanica	P	P
	Gyrosigma/Pleurosigma spp.	P	P
	Licmophora spp.	P	P
	Lyrella clavata	P	P
	Membraneis challengeri	P	P
	Nitzschia spp.	P	P
	cf. *Peronia* spp.	P	-
	cf. *Plagiotropis* spp.	P	P
	Pseudo-nitzschia spp.	P	P
	cf. *Surirella librile*	-	P
	Tabellaria spp.	P	P
	Thalassionema spp.	P	P

Table B2: Dinoflagellate taxa identified in the moored sediment traps at Baie-Comeau (BC-133) and Pointe-des-Monts
480 **(PDM-154 m). P = present in study site. The * symbol highlights thecae/cysts that were not present, but the corresponding theca/cyst was present.**

	Dinoflagellate theca	Dinoflagellate cyst	BC-133	PDM-154
Autotrophic	*Dinophysis acuminata*		P	P
	Dinophysis norvegica		P	P
	Dinophysis spp.		-	P
	Pentapharsodinium dalei	Cyst of *P. dalei**	P	P
	Tripos arcticus		-	P
	Tripos longipes		P	-
Heterotrophic	*Gymnodinium* spp.		-	P
	Protoperidinium americanum*	Cyst of *P. americanum*	P	P
	Protoperidinium bipes		-	P
	Protoperidinium brevipes		P	P
	Protoperidinium conicum*	*Selenopemphix quanta*	P	P
	Protoperidinium minutum?		P	-
	Protoperidinium ovatum		P	P
	Protoperidinium pallidum		P	-
	Protoperidinium pellucidum		-	P
	Protoperidinium spp.	*Brigantedinium* spp.	P	P
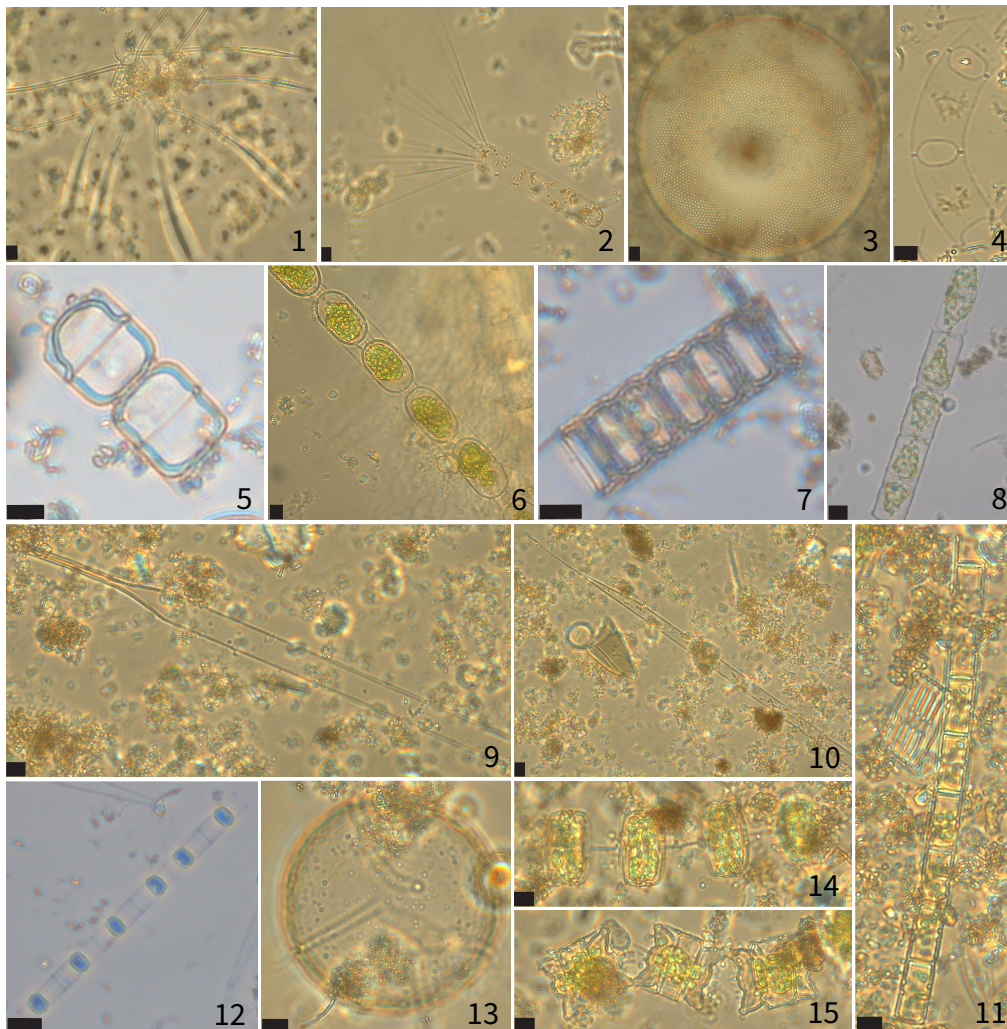
Fig. B1: Micrographs of representative centric diatoms identified in sediment traps BC-133 and PDM-154. 1. *Chaetoceros atlanticus*. 2. *Corethron hystrix*. 3. *Coscinodiscus radiatus*. 4. *Eucampia groenlandica*. 5. *Melosira* spp. 6. *Eupyxidicula turris*. 7. *Paralia sulcata*. 8. cf. *Dactyliosolen fragilissimus*. 9. *Proboscia eumorpha*. 10. *Rhizosolenia hebetata* f. *semispina*. 11. *Detonula confervacea*. 12. *Skeletonema costatum*. 13. cf. *Porosira glacialis*. 14. *Thalassiosira* cf. *gravida*. 15. *Odontella aurita*. All scale bars = 10 µm.

485
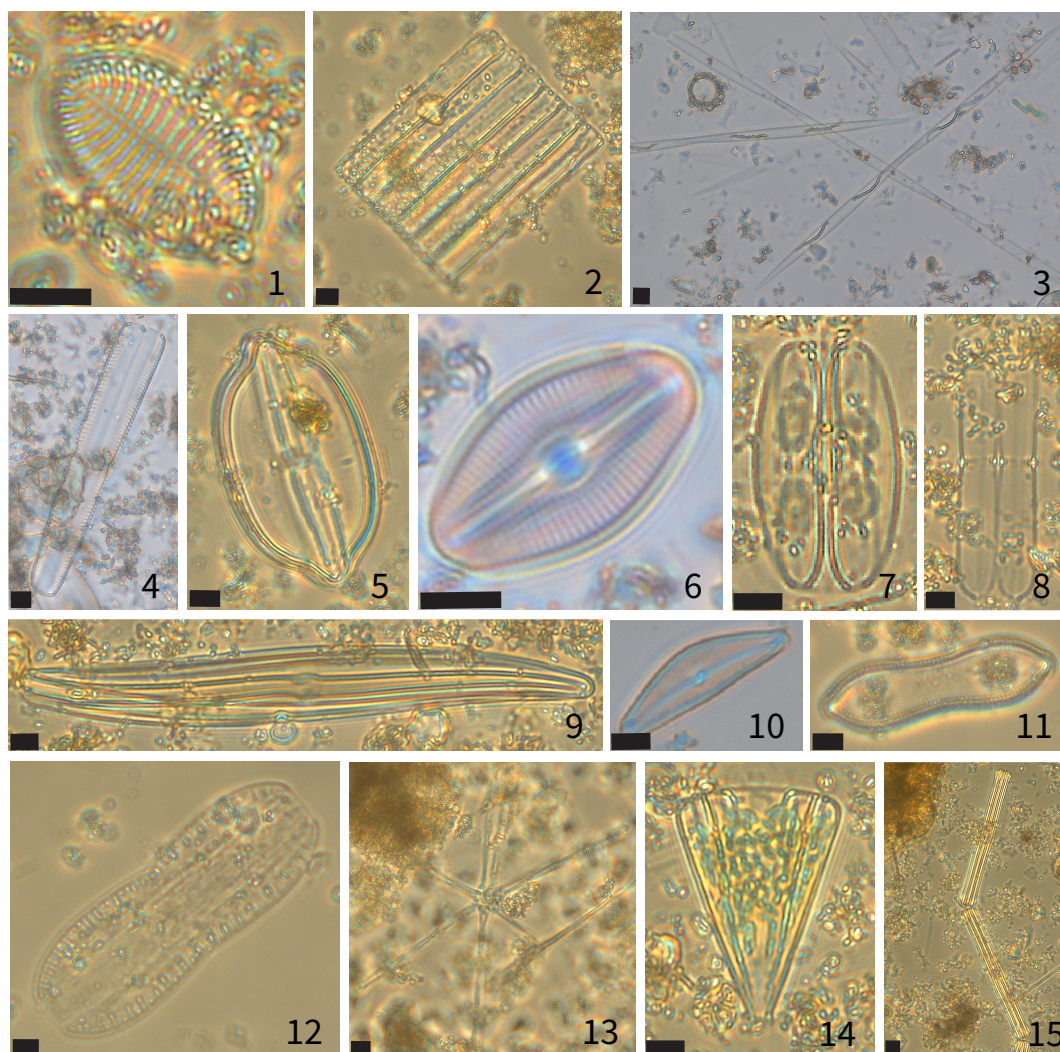
490

Fig. B2: Micrographs of representative pennate diatoms identified in sediment traps BC-133 and PDM-154. 1. *Cocconeis* **spp. 2.** *Nitzschia* **spp. 3.** *Pseudo-nitzschia seriata.* **4. cf.** *Peronia* **spp. 5.** *Lyrella clavata.* **6.** *Diploneis* **spp. 7.** *Membraneis challenger.* **8. cf.** *Plagiotropis* **spp. 9.** *Gyrosigma/Pleurosigma* **spp. 10. cf.** *Epithemia* **spp. 11. cf.** *Surirella librile.* **12.** *Entomoneis* **spp. 13.** *Asterionella* **spp. 14.** *Licmophora* **spp. 15.** *Tabellaria* **spp. All scale bars = 10 µm.**
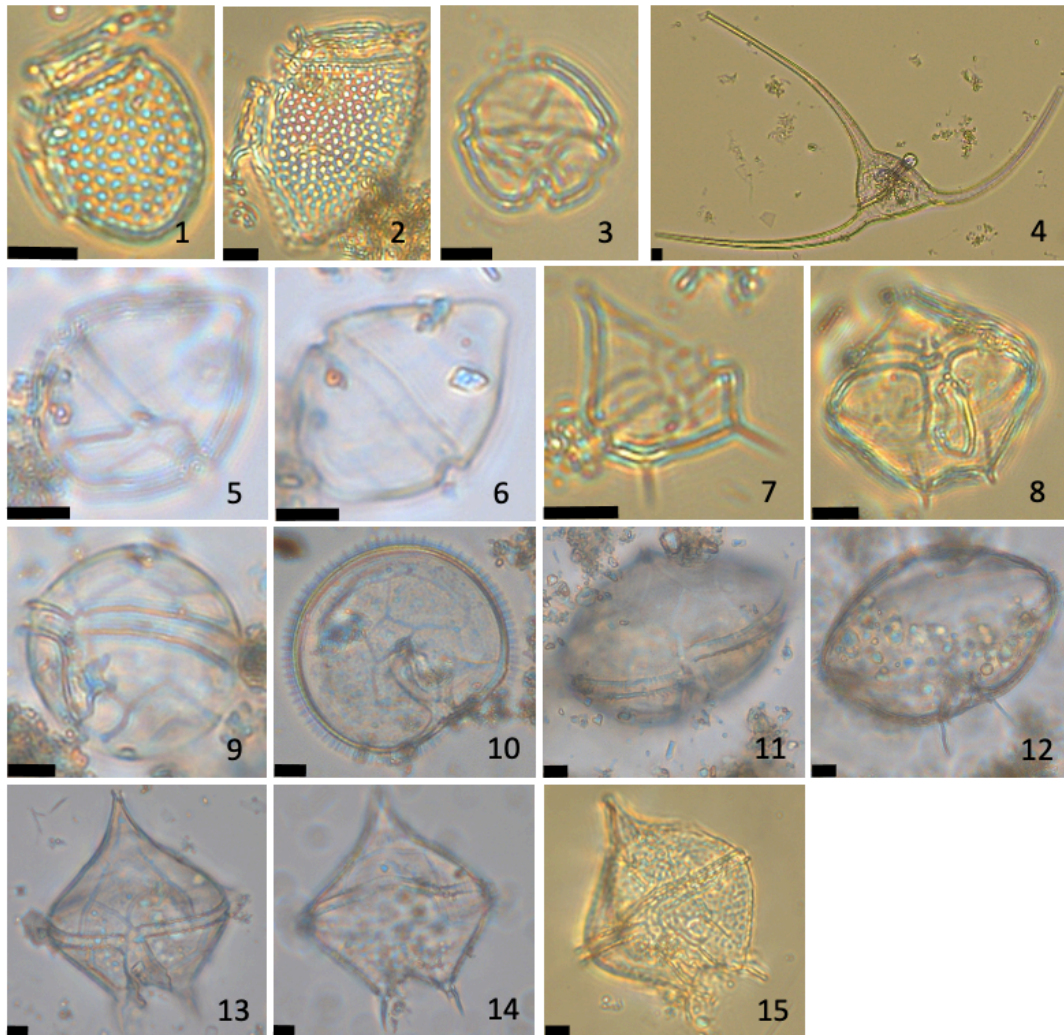
Fig. B3: Micrographs of representative dinoflagellate thecae identified in sediment traps BC-133 and PDM-154. 1.
***Dinophysis acuminata**. 2. **Dinophysis norvegica**. 3. cf. **Gymnodinium** spp. 4. **Tripos arcticus**. 5-6. **Pentapharsodinium dalei**. 7.*
***Protoperidinium bipes**. 8. **Protoperidinium brevipes**. 9. **Protoperidinium minutum?** 10-12. **Protoperidinium ovatum**. 13-14.*
***Protoperidinium pallidum**. 15. **Protoperidinium pellucidum**. All scale bars = 10 μm.*

495

500

505 **Appendix C.**
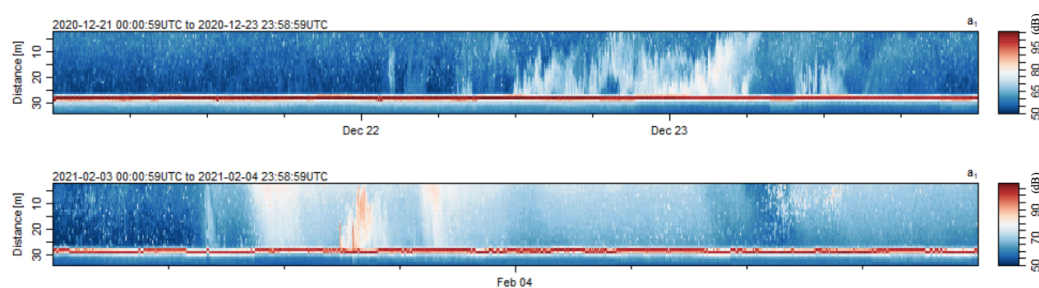
Fig. C1: Backscatter (dB) during the sediment remobilization event (22–23 December 2020) and small turbidity current (3 February 2021) measured using the down-looking Acoustic Doppler Current Profiler in the main axis of the Pointe-des-Monts canyon.

510 **Author contribution**

This project was designed by AL, AN, JCMS, and AL funded the study. HS conducted the analyses and interpretation of the results, prepared the figures, and wrote the original draft of the manuscript with supervision and training from AL, MG, CL, AN, and OS. KB and DB provided the ADCP data. All co-authors contributed to the methodology design, interpretation of the data, and reviewed and approved the manuscript.

515 **Competing interests**

The authors declare that they have no conflict of interest.

Data availability

Data can be accessed through the St. Lawrence Global Observatory.
creators: title, publisher/repository, identifier, publication year (e.g. Loew, A., Bennartz, R., Fell, F., Lattanzio, A.,
520 Doutriaux-Boucher, M., and Schulz, J.: Surface Albedo Validation Sites, EUMETSAT [data set], http://dx.doi.org/10.15770/EUM_SEC_CLM_1001, 2015).

Acknowledgements

This study received financial support from the Marine Environmental Observation, Prediction, and Response Network (MEOPAR) and Réseau Québec Maritime (RQM). We also acknowledge the support of the Natural Sciences and
525 Engineering Research Council of Canada (NSERC-DG 2018-03984 to AL and CGS-M to HS). We thank the participants and crew of the two expeditions on the R/V *Coriolis II*, with special thanks to Christian Boutot for the design, deployment and retrieval of the moorings. We thank Isabelle Tremblay from MEOPAR and Erwann Fraboulet from RQM for their logistical help throughout this project.

References

530   Altabet, M. A., Deuser, W. G., Honjo, S., and Stinen, C.: Seasonal and depth-related changes in the source of sinking particles in the North Atlantic, Nature, 354, 136–139, https://doi.org/10.1038/354136a0, 1991.

Altabet, M. A., and Francois, R.: Sedimentary nitrogen isotopic ratio as a recorder for surface ocean nitrate utilization, Global Biogeochemical Cycles, 8, 10–35, https://doi.org/10.1029/93GB03396, 1994.

Altabet, M. A., and Francois, R.: Nitrogen isotope biogeochemistry of the Antarctic Polar Frontal Zone at 170°W,

535   Deep Sea Research Part II: Topical Studies in Oceanography, 48, 4247–4273, https://doi.org/10.1016/S0967-0645(01)00088-1, 2001.

Bates, S. S., Beach, D. G., Comeau, L. A., Haigh, N., Lewis, N. I., Locke, A., Martin, J. L., McCarron, P., McKenzie, C. H., Michel, C., Miles, C. O., Poulin, M., Quilliam, M. A., Rourke, W. A., Scarratt, M. G., Starr, M., and Wells, T.: Marine Harmful Algal Blooms and Phycotoxins of Concern to Canada, Canadian Technical Report of Fisheries and

540   Aquatic Sciences, Open File 3384, 322 pp., 2020.

Bérard-Therriault, L., Poulin, M., and Bossé, L.: Guide d'identification du phytoplancton marin de l'estuaire et du golfe du Saint-Laurent: Incluant également certains protozoaires, Publication spéciale canadienne des sciences halieutiques et aquatiques, 128, 387 p., 1999.

Bernier, R. Y., Jamieson, R. E., and Moore, A. M.: State of the Atlantic Ocean Synthesis Report, Canadian Technical

545   Report of Fisheries and Aquatic Science, Open File 3167, iii + 149 p., 2018.

Blais, M., Galbraith, P. S., Plourde, S., Devred, E., Clay, S., Lehoux, C., and Devine, L.: Chemical and Biological Oceanographic Conditions in the Estuary and Gulf of St. Lawrence during 2020, Canadian Science Advisory Secretariat Research Document No. 2021/060, iv + 67 p., 2021.

Boivin-Rioux, A., Starr, M., Chassé, J., Scarratt, M., Long, Z., and Lavoie, D.: Harmful algae and climate change on

550   the Canadian East Coast: Exploring occurrence predications of *Dinophysis acuminata*, *D. norvegica*, and *Pseudo-nitzschia seriata*, Harmful Algae, 112, 102183. https://doi.org/10.1016/j.hal.2022.102183, 2022.

Boon, A. R., and Duineveld, G. C. A.: Phytopigments and fatty acids as molecular markers for the quality of near-bottom particulate organic matter in the North Sea, Netherlands Journal of Sea Research, 35, 279–291. https://doi.org/10.1016/S0077-7579(96)90084-8, 1996.

555   Close, H. G.: Compound-specific isotope geochemistry in the ocean, Annual Review of Marine Science, 11, 27–56. https://doi.org/10.1146/annurev-marine-121916-063634, 2019.

Colombo, J. C., Silverberg, N., and Gearing, J. N.L Biogeochemistry of organic matter in the Laurentian Trough, I. Composition and vertical fluxes of rapidly settling particles, Marine Chemistry, 51, 277–293. https://doi.org/10.1016/0304-4203(95)00059-3, 1996.

560   Covault, J. A.: Submarine fans and canyon-channel systems: A review of processes, products and models, Nature Education Knowledge, 3, 2011.

Dickie, L. M., and Trites, R. W.: The Gulf of St. Lawrence, in: Estuaries and Enclosed Seas, edited by Ketchum, B. H., Elsevier., Amsterdam, 403 pp., 1983.

Fernandez-Arcaya, U., Ramirez-Llodra, E., Aguzzi, J., Allcock, A. L., Davies, J. S., Dissanayake, A., Harris, P.,

565   Howell, K., Huvenne, V. A. I., Macmillan-Lawler, M., Martín, J., Menot, L., Nizinski, M., Puig, P., Rowden, A. A.,

Sanchez, F., and Van den Beld, I. M. J.: Ecological role of submarine canyons and need for canyon conservation: A review, Frontiers in Marine Science, 4, 5, doi:10.3389/fmars.2017.00005, 2017.

Fox, A., and Walker, B. D.: Sources and cycling of particulate organic matter in Baffin Bay: A multi-isotope δ^{13}C, δ^{15}N, and Δ^{14}C approach, Frontiers in Marine Science, 9, 846025, doi:10.3389/fmars.2022.846025, 2022.

570   Galbraith, P. S., Chassé, J., Dumas, J., Shaw, J.-L., Caverhill, C., Lefaivre, D., and Lafleur, C.: Physical Oceanographic Conditions in the Gulf of St. Lawrence during 2021, Canadian Science Advisory Secretariat Research Document No. 2022/034, iv + 83 p., 2022.

Genin, F., Lalande, C., Galbraith, P. S., Larouche, P., Ferreyra, G. A., and Gosselin, M.: Annual cycle of biogenic carbon export in the Gulf of St. Lawrence, Continental Shelf Research, 221, 104418,
575   https://doi.org/10.1016/j.csr.2021.104418, 2021.

Gilbert, D., and Pettigrew, B.: Interannual variability (1948–1994) of the CIL core temperature in the Gulf of St. Lawrence, Canadian Journal of Fisheries and Aquatic Sciences, 54, 57–67, https://doi.org/10.1139/f96-160, 1997.

Gilbert, D., Sundby, B., Gobeil, C., Mucci, A., and Tremblay, G.-H.: A seventy-two-year record of diminishing deep-water oxygen in the St. Lawrence estuary: The northwest Atlantic connection, Limnology and Oceanography, 50,
580   1654–1666, doi: 10.4319/lo.2005.50.5.1654, 2005.

Hargrave, B. T., Walsh, I. D., and Murray, D. W.: Seasonal and spatial patterns in mass and organic matter sedimentation in the North Water, Deep Sea Research Part II Topical Studies in Oceanography, 49, 5227–5244, https://doi.org/10.1016/S0967-0645(02)00187-X, 2002.

Hasle, G. R., and Syvertsen, E. E.: Marine Diatoms, in: Identifying Marine Phytoplankton, edited by Tomas, C. R.,
585   Academic Press, 5–385, 1997.

Hwang, J., Manganini, S. J., Montluçon, D. B., and Eglinton, T. I.: Dynamics of particle export on the Northwest Atlantic margin, Deep Sea Research Part I: Oceanographic Research Papers, 56, 1792–1803, https://doi.org/10.1016/j.dsr.2009.05.007, 2009.

Ingram, R. G.: Vertical mixing at the head of the Laurentian Channel, Estuarine, Coastal and Shelf Science, 16, 333–
590   338, https://doi.org/10.1016/0272-7714(83)90150-6, 1983.

Kienast, M., Higginson, M. J., Mollenhauer, G., Eglinton, T. I., Chen, M.-T., and Calvert, S. E. L.: On the sedimentological origin of down-core variations of bulk sedimentary nitrogen isotope ratios, Paleoceanography, 20, PA2009, https://doi.org/10.1029/2004PA001081, 2005.

Lavoie, D., Gilson, G., Chassé, J., Lambert, N., Brunelle, C. B., Starr, M., Plourde, S., Brickman, D., and Maps, F.:
595   Impacts of freshwater flow regulation of Quebec's large rivers on the physical environment and krill transport in the Gulf of St. Lawrence and on the Scotian Shelf, Canadian Technical Report of Hydrography and Ocean Sciences No. 318, xii + 101 p., 2017.

Levasseur, M., Therriault, J.-C., and Legendre, L.: Hierarchical control of phytoplankton succession by physical factors, Marine Ecology Progress Series, 19, 211–222, http://dx.doi.org/10.3354/meps019211, 1984.

600   Macdonald, R. W., Naudi, S. W., and Yunker, M. B.: The Beaufort Sea: Distribution, sources, fluxes and burial of organic carbon, in: The organic carbon cycle in the Arctic Ocean, edited by Stein, R., and Macdonald, R. W., Springer, 177–192, 2004.

Mantoura, R. F. C., and Llewellyn, C. A.: The rapid determination of algal chlorophyll and carotenoid pigments and their breakdown products in natural waters by reverse-phase high-performance liquid chromatography, Analytica

605 Chimica Acta, 151, 297–314, https://doi.org/10.1016/S0003-2670(00)80092-6, 1983.

Mayer, L. M.: Surface area control of organic carbon accumulation in continental shelf sediments, Geochimica et Cosmochimica Acta, 58, 1271–1284, https://doi.org/10.1016/0016-7037(94)90381-6, 1994.

Meyers, P. A.: Preservation of elemental and isotopic source identification of sedimentary organic matter, Chemical Geology, 114, 289–302. https://doi.org/10.1016/0009-2541(94)90059-0, 1994.

610 Minagwa, M., Ohashia, M., Kuramoto, T., and Noda, N.: δ^{15}N of PON and nitrate as a clue to the origin and transformation of nitrogen in the subarctic North Pacific and its marginal sea, Journal of Oceanography, 57, 285–301, https://doi.org/10.1023/A:1012430512137, 2001.

Mucci, A., Starr, M., Gilbert, D., and Sundby, B.: Acidification of Lower St. Lawrence Estuary bottom waters, Atmosphere-Ocean, 49, 206–218, doi:10.1080/07055900.2011.599265, 2011.

615 Nakatsuka, T., Handa, N., Wada, E., and Wong, C. S.: The dynamic changes of stable isotopic ratios of carbon and nitrogen in suspended and sedimented particulate organic matter during a phytoplankton bloom, Journal of Marine Research, 50, 267–296, 1992.

Normandeau, A., Bourgault, D., Neumeier, U., Lajeunesse, P., St-Onge, G., Gostiaux, L., and Chavanne, C.: Storm-induced turbidity currents on a sediment-starved shelf: Insight from direct monitoring and repeat seabed mapping of

620 upslope migrating bedforms, Sedimentology, 67, 1045–1068, doi:10.1111/sed.12673, 2020.

Normandeau, A., Lajeunesse, P., Ghienne, J. F., and Dietrich, P.: Detailed seafloor imagery of turbidity current bedforms reveals new insight into fine-scale near-bed processes, Geophysical Research Letters, 49, e2021GL097389, doi:10.1029/2021GL097389, 2022.

Normandeau, A., Lajeunesse, P., and St-Onge, G.: Submarine canyons and channels in the Lower St. Lawrence

625 Estuary (Eastern Canada): Morphology, classification and recent sediment dynamics, Geomorphology, 241, 1–18, doi: 10.1016/j.geomorph.2015.03.023, 2015.

Normandeau, A., Lajeunesse, P., St-Onge, G., Bourgault, D., Drouin, S. S.-O., Senneville, S., and Bélanger, S.: Morphodynamics in sediment-starved inner-shelf submarine canyons (Lower St. Lawrence Estuary, Eastern Canada), Marine Geology, 357, 243–255, doi:10.1016/j.margeo.2014.08.012, 2014.

630 Parsons, T. R., Maita, Y., and Lalli, C. M.: A Manual of Chemical and Biological Methods for Seawater Analysis, Pergamon Press, 1984.

Paull, C. K., Talling, P. J., Maier, K. L., Parsons, D., Xu, J., Caress, D. W., Gwiazda, R., Lundsten, E. M., Anderson, K., Barry, J. P., Chaffey, M., O'Reilly, T., Rosenberger, K. J., Gales, J. A., Kieft, B., McGann, M., Simmons, S. M., McCann, M., Sumner, E. J., … and Cartigny, M. J.: Powerful turbidity currents driven by dense basal layers, Nature

635 Communications, 9, 4114, https://doi.org/10.1038/s41467-018-06254-6, 2018.

Pilskaln, C. H., Anderson, D. M., McGillicuddy, D. J., Keafer, B. A., Hayashi, K., and Norton, K.: Spatial and temporal variability of *Alexandrium* cyst fluxes in the Gulf of Maine: Relationship to seasonal particle export and resuspension, Deep Sea Research Part II: Topical Studies in Oceanography, 103, 40–54. https://doi.org/10.1016/j.dsr2.2012.11.001, 2014.

640   Redfield, A. C.: The biological control of chemical factors in the environment, American Scientist, 46, 205-221, 1958.

Romero, N., Silverberg, N., Roy, S., and Lovejoy, C.: Sediment trap observations from the Gulf of St. Lawrence and the continental margin of eastern Canada, Deep Sea Research Part II: Topical Studies in Oceanography, 47, 545–583, https://doi.org/10.1016/S0967-0645(99)00118-6, 2000.

Round, F. E., Crawford, R. M., and Mann, D. G.: The Diatoms, Cambridge University Press, 2007.

645   Roy, S., Chanut, J., Gosselin, M., and Sime-Ngando, T.: Characterization of phytoplankton communities in the lower St. Lawrence Estuary using HPLC-detected pigments and cell microscopy, Marine Ecology Progress Series, 142, 55–73, https://doi.org/10.3354/meps142055, 1996.

Ruest, B., Neumeier, U., Dumont, D., Bismuth, E., Senneville, S., and Caveen, J.: Recent wave climate and expected future changes in seasonally ice-infested waters of the Gulf of St. Lawrence, Canada, Climate Dynamics, 46, 449–

650   466, https://doi.org/10.1007/s00382-015-2592-3, 2016.

Ryan, S. A., Wohlgeschaffen, G., Jahan, N., Niu, H., Ortmann, A. C., Brown, T. N., King, T. L., and Clyburne, J.: State of Knowledge on Fate and Behaviour of Ship-Source Petroleum Spills: Volume 4, St. Lawrence Seaway, Montreal to Anticosti, Québec, Canadian Manuscript Report of Fisheries and Aquatic Sciences Technical Report No. 3176, viii + 42 p., 2019.

655   Santora, J. A., Zeno, R., Dorman, J. G., and Sydeman, W. J.: Submarine canyons represent an essential habitat network for krill hotspots in a Large Marine Ecosystem, Scientific Reports, 8, 7579, https://doi.org/10.1038/s41598-018-25742-9, 2018.

Sigman, D. M., Altabet, M. A., McCorkle, D. C., Francois, R., and Fisher, G.: The $\delta^{15}N$ of nitrate in the Southern Ocean: II. Consumption of nitrate in surface waters, Global Biogeochemical Cycles, 13, 1149–1166,

660   doi:10.1006/rwos.2001.0172, 1999.

Steidinger, K. A., and Jangen, K.: Dinoflagellates, in: Identifying Marine Phytoplankton, edited by Tomas, C. R., Academic Press, London, 387–584, 1997.

Therriault, J. C., and Levasseur, M.: Control of phytoplankton production in the Lower St. Lawrence Estuary: Light and freshwater runoff, Naturaliste Canadien, 112, 77–96, 1985.

665   Villanueva, J., and Hastings, D. W.: A century-scale record of the preservation of chlorophyll and its transformation products in anoxic sediments, Geochimica et Cosmochimica Acta, 64, 2281–2294, https://doi.org/10.1016/S0016-7037(99)00428-7, 2000.

Vinyard, W., C.: Diatoms of North America, Mas River Press, Inc., 1979.

Wada, E., and Hattori, A.: Nitrogen isotope effects in the assimilation of inorganic nitrogenous compounds by marine

670   diatoms, Geomicrobiology Journal, 1, 85–101, https://doi.org/10.1080/01490457809377725, 1978.

Walker, B. D., Beaupré, S. R., Guilderson, T. P., McCarthy, M. D., and Druffel, E. R. M.: Pacific carbon cycling constrained by organic matter size, age and composition relationships, Nature Geoscience, 9, 888–891, https://doi.org/10.1038/ngeo2830, 2016.

Waser, N. A. D., Turpin, D. H., Harrison, P. J., Nielson, B., and Calvert, S. E.: Nitrogen isotope fractionation during

675   the uptake and assimilation of nitrate, nitrite, and urea by a marine diatom, Limnology and Oceanography, 43, 215–224, https://doi.org/10.4319/lo.1998.43.2.0215, 1998.

Weise, A. M., Levasseur, M., Saucier, F. J., Senneville, S., Bonneau, E., Roy, S., Sauvé, G., Michaud, S., and Fauchot, J.: The link between precipitation, river runoff, and blooms of the toxic dinoflagellate *Alexandrium tamarense* in the St. Lawrence, Canadian Journal of Fisheries and Aquatic Sciences, 59, 464–473, https://doi.org/10.1139/f02-024,
680   2002.